J-QE/28/10//01990

Simplified Characterization of Uniaxial and Biaxial Nonlinear Optical Crystals: A Plea for Standardization of Nomenclature and Conventions

David A. Roberts

Reprinted from
IEEE JOURNAL OF QUANTUM ELECTRONICS
Vol. 28, No. 10, October 1992

POST-PUBLICATION AUTHOR COMMENTS ..... December, 1992:

1. Some readers have indicated confusion regarding the direction cosines b_{ij} in (27)-(28) for optical-eigenmode electric field vectors **E**. As stated on pp. 2065 and 2066, one can obtain these b_{ij} from the eigenmode **D**-polarization direction cosines a_{ij} by substituting the **S**,**E** direction cosine angles in (23)-(25) for the respective **k**,**D** angles in (1). The confusion apparently centers on the requirement for substitution into (1b) a slightly different polarization parameter (25b) than the parameter (25a) that is substituted into (1a). This just reflects that, while the two eigenmode **D**-polarizations at each λ_1 are inherently orthogonal, and can therefore be characterized by a single polarization parameter δ_1 in (1), the two **E**-polarizations are not mutually orthogonal in the general biaxial case. The **E**'s at m=1 and m=2 therefore have to be characterized by slightly different polarization parameters (25a) and (25b), respectively, which give orthogonal **E**'s at each λ_1 only for uniaxial and/or principal plane propagation.

2. The ratio d_{31}/d_{32} for $KNbO_3$, reported as negative in [30]-update, should have been reported as positive, in contradiction to [27] but in agreement with [28]. This positive ratio has been reaffirmed by very recent, unpublished measurements by B. Zysset (Sandoz, France) and also by K. Kato (Japan Defense Agency). Thus, the coefficient d_{32} ($=d_{24}$) in our Table VI should be negative. Thanks to I. Biaggio (Swiss Federal Institute of Technology) for bringing this matter to my attention.

3. The KTP nonlinear coefficients kindly given to this author as an update to reference [31] were later adjusted by authors H. Vanherzeele and J. D. Bierlein just prior to publication in Optics Letters, vol. 17, No. 14, pp. 982-984, 1992. These adjustments were small, however, and do not materially affect the recommended standard values for these coefficients given in our Tables V and VI.

4. A typographical error in the published IEEE/JQE version of Table V, $AgGaS_2$ at 10.6μm, reads "1.1/CMD from 1.064μm average". The incorrect figure "1.1" has been corrected in this reprint to "11.1". This is an excellent example of the efficacy of Miller's Rule in predicting dispersion in the optical nonlinear coefficients, in this case a 37% decrease in d_{36} for an order-of-magnitude increase in SHG wavelengths.

Simplified Characterization of Uniaxial and Biaxial Nonlinear Optical Crystals: A Plea for Standardization of Nomenclature and Conventions

David A. Roberts, *Member, IEEE*

Abstract—**Lack of adherence to uniform nomenclature and conventions in nonlinear crystal optics has resulted in growing confusion within the industry and its literature. We propose standards which eliminate ambiguity in reporting nonlinear phenomena, especially in the increasingly complex realm of biaxial crystals. In order to restore uniformity to the designation of crystallographic axes and crystal tensor properties (such as the nonlinear coefficients), we recommend the adoption of IEEE/ANSI Std. 176, with a small but much needed modification for crystal class mm2, as recommended to IEEE and discussed herein. For the reporting of nonlinear interaction characteristics, other frames are proposed which result in simpler rules than heretofore given for categorizing phase-matching loci, and for characterizing eigenmode polarizations, double refraction, effective nonlinear coupling, and first- and second-order acceptance bandwidths (angular, spectral, thermal) along these loci. Similarities as well as differences between biaxial and uniaxial crystals are emphasized. Finally, a comprehensive, self-consistent set of nonlinear coefficients for large and small band-gap materials is given in order to facilitate more realistic NLO figure-of-merit comparisons among different crystals.**

I. Introduction

THE discovery of optical second harmonic generation (SHG) in 1961, coupled with more recent advances in laser technology and applications theory, has led to increasingly rapid progress in the field of nonlinear optics [1], [2]. Until recently, the field of nonlinear optics (NLO) was restricted primarily to uniaxial crystals, where the need for crystallographic nomenclature and convention was modest. Now, with increasing interest in biaxial crystals and more broadly based participation, there is a growing lack of uniformity in the literature regarding nomenclature, convention standards, and frames of reference with which theoreticians and experimentalists analyze, report, and compare their works.

We propose a uniform approach to the reporting of sum/difference frequency mixing (SFM/DFM) and parametric interactions (OPO/OPA) in NLO crystals, independent of axiality or class. This approach, for the most part, would utilize standards and de facto standards already in place, but not uniformly adhered to. We shall first discuss frames of reference currently in use, as well as problems which arise when these frames are not clearly stated or when there is conflicting use of symbols designating these frames. From these, we shall recommend specific standardized frames for reporting tensor quantities (such as nonlinear coefficients), and others for directions of beam propagation, polarizations, and walkoff. These frames should suit the needs of NLO theoreticians, experimentalists, and crystal manufacturers alike. We outline computational approaches and characterizations of biaxial crystals in these frames, using a physically intuitive approach which is directed towards the broadest possible readership and which underscores both the similarities and differences between biaxial and uniaxial crystals. Finally, we propose an updated absolute scale for nonlinear coefficients for both large and small band-gap materials. This makes possible more uniform and more realistic comparisons of NLO behavior, as will be demonstrated for crystals of current and recent interest.

Manuscript received November 17, 1991; revised June 2, 1992.

The author is with Cleveland Crystals, Inc., Highland Heights, OH 44143.

IEEE Log Number 9201990.

II. Convention/Nomenclature Overview

The first formal, comprehensive standard designating natural axes and rectangular reporting frames in crystalline materials was published in the *Proceedings of the IRE* in 1949 [3], and subsequently became IEEE Std. 176-1949. This set of conventions and nomenclature was created by a consensus of expertise in crystallography, physics, and engineering in order to standardize the reporting of tensor material properties for crystal mechanics, acoustics, dielectrics, and piezoelectrics, all interrelated through the tensor constitutive equations of piezoelectricity. This standard has been revised and augmented over the years to meet evolving needs for unambiguous sign conventions, tensor subscript notation, and strict right-handedness of reporting frames, including accommodation of both left- and right-hand forms of enantiomorphous materials such as quartz. The current version of this standard is IEEE/ANSI Std. 176-1987 [4], and was approved by the IEEE Standards Board and the American

National Standards Institute (ANSI) in 1987, reaffirming, for the most part, the previous version, IEEE/ANSI Std. 176-1978. Current IEEE Board policy mandates further review and update (if necessary) every five years. A brief summary of conventions of interest to practitioners of nonlinear optics is given in Appendix IV.

It is apparent from the literature that the early (1949) IRE/IEEE conventions became a de facto standard for crystallographic nomenclature and the reporting of nonlinear coefficients in nonlinear optics, at least until the relatively recent rise to prominence of biaxial crystals. The use of Std. 176 is particularly appropriate because crystal classes which exhibit piezoelectric properties are the same (acentric) classes which exhibit NLO effects. Although NLO effects benefit from additional symmetries (inversion, Kleinman) over those for piezoelectric effects [5], similar powerful symmetry arguments apply, as we shall see. Coupling of mechanical, piezoelectric, and NLO effects imposed by thermal loading in high-average power applications [52], [53] and/or electrooptic tuning of birefringence [54] has heightened the need for convention standardization for all of these diverse but potentially interacting disciplines.

III. Standard Frames of Reference

IEEE/ANSI Std. 176 definitions of natural crystallographic axes *abc* are summarized in Appendix IV. Since these axes are not necessarily mutually orthogonal, Std. 176 also defines right-handed, rectangular frames (upper case) *XYZ* for more convenient reporting of (tensor) crystallographic properties. As indicated in Appendix IV, the *XYZ* axes are closely related to axes *abc* and/or prominent crystallographic planes, and also have unequivocal polarity assignments [4]. Because of the similar relationships of nonlinear optical coefficients d_{ijk} (m/V) and piezoelectric coefficients d_{ijk} (m/V) to crystal symmetry, it has been traditional to report both in the *XYZ* system, but there has been a problem in this regard for the polar orthorhombic class, as we shall describe shortly.

The IEEE/ANSI standard defines "any other rectangular frame" to be $x_1x_2x_3$, but (lower case) *xyz* has traditionally been used for the principal optical axes [10], [13], [14]. Although the *xyz* and *XYZ* frames both happen to be spatially coincident with the principal dielectric axes in uniaxial and orthorhombic crystal classes, they are defined differently, as we shall see. For orthorhombic crystals in particular, there is no *a priori* relationship between specific axes in the two frames, such as exists for uniaxial negative crystals ($x = Z$) and uniaxial positive crystals ($z = Z$). Such relationships must be determined experimentally. For monoclinic and triclinic classes, the relationship between *xyz* and *XYZ* frames is more complex and also subject to dispersion (see example in Appendix III), so that those who publish in the NLO literature should also specify the dispersive relationship of the frame *xyz* to the unequivocal frame *XYZ*.

IV. Problems with Concurrent Frames (and proposed solution)

Problems arising from the concurrent use of the three reference frames *abc*, *XYZ*, and *xyz* are severalfold, not the least of which is that the literature too often fails to communicate which is being used or how the *xyz* frame is related to the *abc*/*XYZ* frames. This problem is compounded by indiscriminate use of lower/upper-case designations for frames *xyz*/*XYZ*. Also, axes *xyz* have occasionally been designated by $\alpha\beta\gamma$ (an old crystallographers' convention), even though both the IRE and the IEEE/ANSI standards reserve the symbols α, β, γ for crystallographic interaxial angles. Other custom frames have also been used. For instance, *Y* (rather than *X*) has occasionally been associated with the normal to both *c* and one of the three equivalent mirror planes containing *c* in trigonal class 3m (BBO, $LiNbO_3$). In such cases, the IEEE/ANSI nonlinear coefficient d_{22} is then reported as d_{11}, etc.

Adding to the foregoing problems is the occasional use of left-handed versions of the above reference frames, leading to relative signs for the nonlinear coefficients which may differ from those appropriate to right-hand conventions. Assuming Kleinman's symmetry conjecture applies [5], this occurs only for the sign of $d_{14} = d_{25} = d_{36}$ with respect to any other nonzero coefficients in triclinic 1, monoclinic 2, and tetragonal $\bar{4}$ classes. In such cases, the use of left-handed reporting frames for the d_{ijk} invites miscalculation of effective (net) nonlinear couplings d_{eff} [59] by those who are used to following right-hand conventions. For example, the negative d_{25} coefficient reported for *d*-LAP in [18] would be positive in the corresponding right-handed frame (see Appendix III), and has been updated as such by the authors in [19].

In order to promote awareness of and distinction among the different frames *abc*, *xyz*, and *XYZ*, we encourage that coordinate axes and refractive indexes be given multiple designations, such as $x = c = Z$ and $n_{x=c}$, or whatever is appropriate (see also monoclinic example, Appendix III). This practice would also minimize potential confusion between lower/upper case designations *xyz*/*XYZ*.

V. Convention Anarchy: Orthorhombic mm2

Despite the thoughtful development of Std. 176 over many years, the polar orthorhombic crystal class has been an anathema in the quest for industry standardization. This is the one orthorhombic class (from a total of three) that has a unique, polar, twofold axis. The original IRE Std. defined the unit cell axes as $c_o < a_o < b_o$, then equated $X = a$, $Y = b$, and $Z = c$. Unfortunately, this implicitly required that there be three permutations of the *XYZ* frame for tensor quantities, such as the d_{ijk}, depending on whether the twofold axis is *a*, *b*, or *c*. This oversight was rectified in IEEE/ANSI Std. 176-1978 (and reaffirmed in Std. 176-1987) by defining the polar axis as *Z*. The current standard retains the unit cell convention $c_o < a_o < b_o$, but *X* now designates the shorter of the two nonpolar

TABLE I
IEEE/ANSI-STD. 176-1987 AND LITERATURE AXIS/CLASS DESIGNATIONS IN ORTHORHOMBIC CRYSTALS HAVING A SINGLE TWOFOLD AXIS (ALL FRAMES RIGHT-HANDED)

Crystal [ref]	IEEE/ANSI M	L	S	Class	Literature M	L	S	Class	Difference
BTCC	Z	Y	X		X	Z	Y		Axes a, b, X, Y, Z;
	a	b	$-c$	2mm	b	a	c	mm2	d12, 13, 11, 26, 35 =
[22]	x	z	y		x	z	y		IEEE d31, 32, 33, 15, 24.
GMO	Y	Z	X		Y	Z	X		
	a	b	c	m2m	b	c	a	mm2	Axes a, b, c only
[23]	x	z	$-y$		x	z	$-y$		
KB5	X	Y	Z		X	Y	Z		none, but fortuitous
	a	b	c	mm2	a	b	c	mm2	(intent was $Z = c$ = polar
[24]–[26]	z	$-y$	x		z	$-y$	x		de facto convention)
$KNbO_3$	Y	Z	X		X	Z	Y		b, c, X, Y;
	a	b	c	m2m	a	c	b	mm2	d_{31}, d_{32} reversed from
[27], [28]	$-y$	x	z		y	x	z		IEEE (same for d_{15}, d_{24}).
KTP/KTA	Z	Y	X		Z	X	Y		a, b, c, X, Y;
	a	b	$-c$	2mm	c	a	b	mm2	d_{31}, d_{32} reversed from
[29]–[32]	z	x	$-y$		z	x	y		IEEE (same for d_{15}, d_{24}).
LBO	X	Y	Z		Y	X	Z		a, b, X, Y
	a	b	c	mm2	b	a	c	mm2	d_{31}, d_{32} reversed from
[33]–[37]	z	x	y		z	x	$-y$		IEEE (same for d_{15}, d_{24}).
LFM	X	Y	Z		X	Y	Z		none, but fortuitous
	a	b	c	mm2	a	b	c	mm2	(intent was $Z = c$ = polar
[38], [39]	x	y	z		x	y	z		*de facto* convention)
ZTS	Y	Z	X		Y	Z	X		xyz used for XYZ.
	a	b	c	m2m	$-a$	c	b	mm2	Axes b, c reversed.
[40]	y	z	x		y	z	x		$\alpha\beta\gamma$ used for xyz.

The literature largely conforms to the *de facto* standard "$Z = c$ = polar," but only in part to $X = a$ as the shorter nonpolar axis (the BTCC literature designation "mm2" is inconsistent with "polar = b"). Our proposed Std. 176 amendment changes IEEE designations abc, not XYZ.

axes, and Y is chosen to give right-handed frame XYZ. Unfortunately, the current standard has resulted in the somewhat clumsy class designation 2mm, m2m, or mm2, depending on whether the twofold axis is a, b, or c. Also, many crystallographic and NLO publications prior to and since the 1978 revision still reference the original IRE Std. [6], [13], while relatively few works [8] reference the IEEE/ANSI updates. Other publications [7], [12] use mixed or different conventions.

It is therefore apparent that IEEE/ANSI Std. 176 conventions for the polar orthorhombic class have not received widespread acceptance by the crystal physics and engineering communities, which use, instead, an older (de facto) standard that designates the twofold axis as both c and Z [12]. This reflects the desire to have the highest symmetry axis labeled as c (the practice used for uniaxial crystals), but it has not been formalized as part of a more comprehensive standard, and those who use it are not agreed on how to define a, b, X, or Y. The IRE and IEEE/ANSI convention $c_o < a_o < b_o$ reflects the desire of mineralogists to identify c with the unique morphological axis, which is often, though unreliably, associated with the short unit cell dimension.

Table I compares crystallographic axes abc, tensor reporting frame axes XYZ, and principal optical axes xyz for several polar orthorhombic crystals in the nomenclature of both IEEE/ANSI Std. 176-1987 and the literature, using the small, medium, and large unit cell dimensions (denoted by S, M, and L) as an unequivocal spatial reference. The occasional negative axis designation in Table I is necessary for right-handedness of frames abc and xyz relative to right-handed $+X$, $+Y$, $+Z$ (unequivocal polarities defined in [4]). The axis for such negative designation is otherwise arbitrary, but we prefer y and/or its associated a, b, or c axis.

For polar orthorhombic crystals, it is apparent from Table I that "$Z = c$ = polar," not IEEE/ANSI Std. 176, approaches a *de facto* standard in the NLO literature. Ordinarily, we would enthusiastically support a comprehensive, well-documented, widely distributed, and (for the most part) widely accepted standard, such as IEEE/ANSI Std. 176. It is, in our opinion, currently the only standard that fulfills all of these criteria, and it is certainly a very workable one, despite the awkwardness of and anarchy over orthorhombic mm2. However, we also believe that a good standard should reflect common practice, especially if that practice has greater merit. Hence, we have recommended to the IEEE Subcommittee on Piezoelectric Crystals that Std. 176 be amended in the next update (tentatively scheduled for 1992) to support the polar orthorhombic de facto standard "$c = Z$ = polar," with $a = X$ chosen such that $a_o < b_o$, and with $b = Y$ chosen to give right-hand frames abc and XYZ. This restores the older IRE single designation mm2 for all crystals in this class,

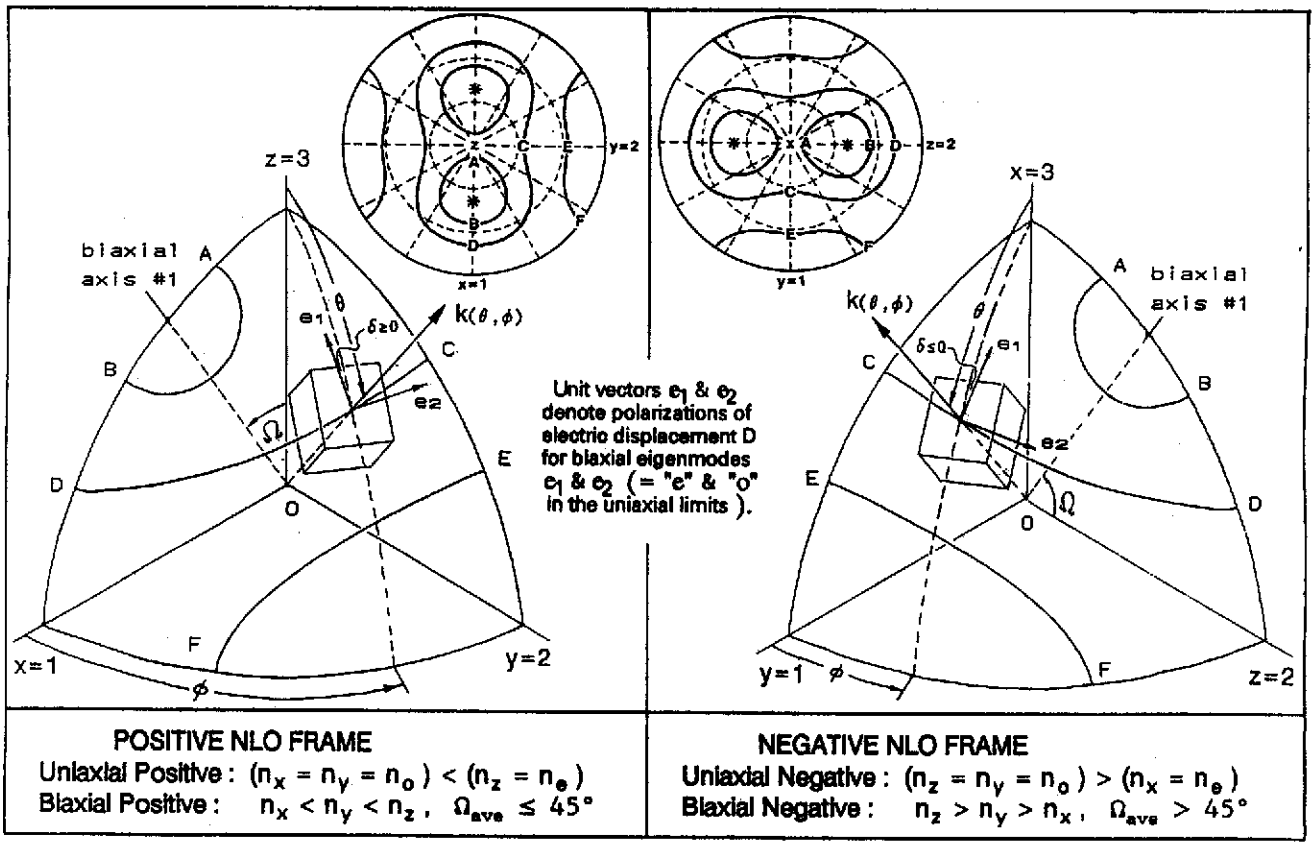

(a) (b)

Fig. 1. 1st Octant (+ optional 4-octant stereonet) of proposed positive and negative NLO reporting frames.

eliminates the possibility that $-a$, $-b$, or $-c$ can be associated with $+X$, $+Y$, or $+Z$, and leaves unchanged the current Std. 176 XYZ frame definition and $a_o < b_o$ axis relation. Our recommendation has been well received and is being actively considered as of this writing.

VI. Proposed NLO Reporting Frames (Return to Uniaxial Tradition)

The calculation of wave normal directions for phase-matched propagation in a NLO crystal can be accomplished by using a mathematical construction called the optical indicatrix, an ellipsoid in the xyz frame with semi-axes equal to refractive indexes n_x, n_y, n_z. Fig. 1 illustrates a crystal in the first octant thereof, along with normal-incidence wave vector $\boldsymbol{k}$. Only normal-incidence, collinear beams are considered here (noncollinear beams are treated, e.g., in [17]). The angles θ, ϕ used in the literature to report the direction of $\boldsymbol{k}$ are not always given as spherical coordinates with respect to the xyz frame. In particular, for negative uniaxial crystals, θ is conventionally (and conveniently) measured from the optic axis, which is x rather than z. This confusing situation is easily rectified by defining a standard NLO reporting frame 123 which is either a "positive NLO frame" [123 = xyz, Fig. 1(a)] or a "negative NLO frame" [123 = yzx, Fig. 1(b)]. The familiar uniaxial angular coordinates θ, ϕ are then conventional spherical coordinates in this 123 system. For uniaxial crystals only, the "3" axis always corresponds to the unique "optic axis," which is crystallographic axis c and XYZ tensor reporting frame axis Z.

We propose that the above-defined NLO reporting frames be adopted as standard for all crystals, uniaxial, and biaxial. The positive/negative NLO frame should be used for positive/negative uniaxial crystals, in keeping with uniaxial tradition. For biaxial crystals, the appropriate choice may seem less clear. Although biaxial crystals have been classified in optics and mineralogy texts as birefringent "positive" or "negative" [15], [16], these designations are usually avoided in the NLO literature, probably because there is no abrupt transition in NLO characteristics near $n_y = (n_x + n_z)/2$ or $\Omega = 45°$ in Fig. 1 (strictly equivalent conditions only in the limit of vanishing birefringence). In a marginal case, a biaxial crystal could be considered both positive and negative, depending on index dispersion over the three wavelengths λ_i (i = 1, 2, 3) in the interaction. The appropriate NLO reporting frame in these marginal situations is therefore somewhat arbitrary. We recommend as a standard for a biaxial "positive" crystal that average $\Omega \leq 45°$, and for a biaxial "negative" crystal that average $\Omega > 45°$.

For any direction of propagation $\boldsymbol{k}$ within the crystal there are two eigenmodes, generally known as "fast" and "slow," with equal propagation speeds only when $\boldsymbol{k}$ is

directed along an optic axis (a case not normally of practical interest). In Fig. 1, mutually orthogonal unit polarization vectors e_1 and e_2 are parallel to eigenmode electric displacements D inside the crystal (also electric fields E outside the crystal, assuming normal incidence) [14]. Knowledge of their orientations with respect to the crystal surfaces is required in order to set correct input polarization(s).

The significance of the optical indicatrix in Fig. 1 is that if e_1 (or e_2) is polarized along x, y, or z, the wave has a phase velocity determined by corresponding index n_x, n_y, or n_z. The phase velocity of an eigenwave with general polarization is a geometric function of all three indexes [13], [14]. In a nondegenerate three-wave interaction, there are three such indicatrices, one for each wavelength. Their like semiaxes are spatially coincident (except for monoclinic and triclinic crystals) and differ in lengths only by dispersion. Sections containing the common origin "O" and normal to k define three ellipses. Their major/minor semiaxes denote the electric displacement directions and the magnitude of the net refractive indexes for the slow/fast eigenmodes, respectively. In Fig. 1, we define e_1, e_2 as the slow, fast eigenmodes if the POSITIVE NLO FRAME is used, and as the fast, slow eigenmodes if the NEGATIVE NLO FRAME is used. This ensures that e_1 and e_2 correspond to traditional eigenmodes "e" and "o" in the uniaxial limits, where $\delta = 0$. This correspondence to the more familiar and traditional uniaxial case, as a point of departure, facilitates straightforward generalizations about the detailed behavior of the more complex biaxial eigenmodes, as we will demonstrate later.

VII. Loci of Phase-Matched Propagation (Simplified Categorization)

It is well known that wave normals $k(\theta, \phi)$ for phase-matched propagation in uniaxial positive and negative crystals intersect the optical indicatrices in circular loci around the optic axes, z and x, respectively. Biaxial loci, on the other hand, are of three types, which we designate by AB, CD, and EF in Fig. 1, where loci in the remaining seven octants can be obtained by successive mirror reflections of first octant loci across the principal optical planes. We believe that this three-locus method of categorizing biaxial phase-matching loci is easier to characterize and remember than the 21 categories enumerated by Hobden [42]. For the illustration of such loci, we favor a four-octant stereonet similar to the one used by Velsko (Fig. 1 insets), with optional peak and valley designations of d_{eff}^2 or other NLO figure-of-merit along the loci, indicating optimum phase-matching directions and the effects of crystal symmetry thereon [44]. In the following sections, we will characterize biaxial polarizations, walkoff, etc., along the three loci in our POSITIVE and NEGATIVE NLO FRAMES, and compare with uniaxial characteristics.

One approach to solving for the allowed loci θ, ϕ in biaxial crystals is to start from the Fresnel equations for wave normals [14]. These are characteristic value equations whose two solutions at a given wavelength are the indices of refraction for the two eigenmodes $m = 1, 2$. Yao and Fahlen [46] have shown how Fresnel's equations can be manipulated to yield relatively simple transcendental equations in θ and ϕ. These can then be iteratively solved for the θ, ϕ loci for a given set of interaction wavelengths. Although Yao and Fahlen have explicitly addressed only Type I and II SHG in positive crystals, their results are easily generalized to Type I/II/III SFM, DFM, OPO, and OPA, in both positive and negative crystals (see Appendix II and/or [49]).

TABLE II
POTENTIALLY PHASE-MATCHABLE COMBINATIONS OF e_1 AND e_2 EIGENMODES FOR BIREFRINGENT POSITIVE AND NEGATIVE CRYSTALS IN THE APPROPRIATE FIG. 1 NLO REPORTING FRAME, WHERE $\lambda_1 \geq \lambda_2 > \lambda_3$

Polz Type	SHG, SFM In	SHG, SFM Out	DFM_{32}, OPA_{32} In	DFM_{32}, OPA_{32} Out	DFM_{31}, OPA_{31} In	DFM_{31}, OPA_{31} Out	OPO In	OPO Out
	$\lambda_1, \lambda_2 \rightarrow \lambda_3$		$\lambda_3, \lambda_2 \rightarrow \lambda_1$		$\lambda_3, \lambda_1 \rightarrow \lambda_2$		$\lambda_3 \rightarrow \lambda_1, \lambda_2$	
I^+	$e_1, e_1 \rightarrow e_2$		$e_2, e_1 \rightarrow e_1$		$e_2, e_1 \rightarrow e_1$		$e_2 \rightarrow e_1, e_1$	
I^-	$e_2, e_2 \rightarrow e_1$		$e_1, e_2 \rightarrow e_2$		$e_1, e_2 \rightarrow e_2$		$e_1 \rightarrow e_2, e_2$	
II^+	$e_2, e_1 \rightarrow e_2$		$e_2, e_1 \rightarrow e_2$		$e_2, e_2 \rightarrow e_1$		$e_2 \rightarrow e_2, e_1$	
II^-	$e_1, e_2 \rightarrow e_1$		$e_1, e_2 \rightarrow e_1$		$e_1, e_1 \rightarrow e_2$		$e_1 \rightarrow e_1, e_2$	
III^+	$e_1, e_2 \rightarrow e_2$		$e_2, e_2 \rightarrow e_1$		$e_2, e_1 \rightarrow e_2$		$e_2 \rightarrow e_1, e_2$	
III^-	$e_2, e_1 \rightarrow e_1$		$e_1, e_1 \rightarrow e_2$		$e_1, e_2 \rightarrow e_1$		$e_1 \rightarrow e_2, e_1$	

e_1, e_2 ("e" and "o" in the uniaxial limit) are the slow, fast eigenmodes for positive crystals and the fast, slow eigenmodes for negative crystals. Hence, fast and slow assignments for respective waves $i = 1, 2, 3$ are identical for positive and negative crystals, and λ_3 is always the fast eigenmode.

An alternate, but equivalent, approach for determining the allowed θ, ϕ loci uses the Fig. 1 indicatrix construction to determine net refractive indexes for the eigenmodes $m = 1, 2$, given the directions of their polarizations D (implicit in the approach discussed above). Ito [47] has given direction cosines $a_{ij}^{(m)}$ describing these e_1, e_2 polarizations, as given in (1a) and (1b) below. However, he incorrectly identifies the direction cosines with internal fields E rather than displacements D, resulting in a lack of walkoff corrections in his d_{eff} calculations. This point will be discussed in more detail in Sections X and XI. Note that we have made corrections for the typographical errors in [47] and the addition of wavelength subscripts i to account for dispersion in these direction cosines, plus accommodation to the right-hand rule ($+\delta$ is clockwise looking along k, or counterclockwise looking down k towards the origin "O" in Fig. 1).

$$a_{ij}^{(1)} = \begin{pmatrix} -\cos\theta\cos\phi\cos\delta_i + \sin\phi\sin\delta_i \\ -\cos\theta\sin\phi\cos\delta_i - \cos\phi\sin\delta_i \\ +\sin\theta\cos\delta_i \end{pmatrix} \quad \text{(1a)}$$

$$a_{ij}^{(2)} = \begin{pmatrix} -\cos\theta\cos\phi\sin\delta_i - \sin\phi\cos\delta_i \\ -\cos\theta\sin\phi\sin\delta_i + \cos\phi\cos\delta_i \\ +\sin\theta\sin\delta_i \end{pmatrix}. \quad \text{(1b)}$$

Calculation of the angles δ_i is discussed in the next section. Ito follows the traditional practice of associating e_1, e_2 with the slow and fast eigenmodes, by identifying δ with the angle between the polarization e_1 and the plane of k and the z axis. As stated previously, however, we feel that greater simplification results in the perception and categorization of biaxial behavior from associating e_1, e_2 with respective uniaxial counterparts "e" and "o". Hence, at each wavelength λ_i, we identify δ_i in (1) and Fig. 1 with the angle between the polarization e_1 and the plane of k and the Fig. 1 "3"-axis. This gives the desired result that the δ_i are identically zero in the uniaxial limit for both positive and negative crystals.

Starting with the traditional (vacuum) wavelength convention $\lambda_1 \geq \lambda_2 > \lambda_3$, the Fig. 1 θ, ϕ loci can be determined by the usual phase-matching conditions [13]:

$$\Delta k = 2\pi n_3/\lambda_3 - 2\pi n_2/\lambda_2 - 2\pi n_1/\lambda_1 = 0 \quad (2)$$

$$1/\lambda_1 + 1/\lambda_2 = 1/\lambda_3 \quad (3)$$

where

$$n_i^{(m)} = \left[\sum_{j=1}^{3} [(a_{ij}^{(m)})/n_{ij}]^2\right]^{-1/2}. \quad (4)$$

Unless indicated otherwise in this paper, we use a single subscript to denote wave $i = 1, 2, 3$, and a double subscript ij to denote, additionally, a component along axis $j = 1, 2, 3$, ($= x, y, z$ or y, z, x in Fig. 1). Hence, the n_{ij} in (4) are (vacuum) wavelength dependent refractive indexes, and the $n_i^{(m)}$ designate the net indexes of refraction n_i in (2) which depend, additionally, on the appropriate polarization assignments ($m = 1$ or 2), as well as the wave normal direction θ, ϕ and Fig. 1 polarization angles δ_i. There are eight combinations of eigenmodes $m = 1, 2$ taken three at a time in (2), but only six are potentially phase matchable via the traditional technique of compensating phase-velocity dispersion by angle, temperature or electrical tuning of natural birefringence. They are traditionally designated polarization Type I (λ_1, λ_2 polarizations the same) and Type II (λ_1, λ_2 polarizations different) [41], [42], which unfortunately does not distinguish between the two possible permutations of λ_1, λ_2 polarization assignments in Type II interactions. This was recognized by Eimerl [43], who has designated the more familiar assignments by Type II (consistent with previous tradition) and the less familiar assignments by Type III, as summarized in Table II. We recommend that this nomenclature be adopted as standard.

In spite of the numerous applications indicated in Table II, it is necessary to know only the sign of the birefringence and the polarization type in order proceed with the solution for phase-matched wave normal directions θ, ϕ in (2). The interaction type is irrelevant. The number of iterations for solutions θ, ϕ will depend on the accuracy desired, the sophistication of the algorithm, and the particular θ, ϕ location on the phase-matching locus.

The exact shape and location of the Fig. 1 loci depend on polarization type and indexes of refraction. There is no assurance that there will be a solution for all (or even any) of the three locus types AB, CD, or EF for a given set of wavelengths. It is not uncommon, however, that at least two of these locus types are represented among the numerous combinations of polarization types (I/II/III) and wavelengths in a crystal's transmission band. This is more likely for larger biaxiality, i.e., for Ω significantly different from the uniaxial values 0° and 90° in Fig. 1, and for larger birefringence. Type III generally has the smallest (if any) spectral range of phase matchability, which explains why it has often been ignored in the literature. The possibility that Type III may have the best NLO figure-of-merit for a given interaction should not be a priori dismissed, however, especially since it often has the largest angular acceptance bandwidth. This will be illustrated later when we discuss example reporting of NLO interactions in Table VII.

Having determined a phase-matching locus of interest, we note that the sensitive and insensitive angle-tuning planes are normal and tangent, respectively, to this locus. In Fig. 1, skewness of a locus to the crystal side faces (zero at locus points A through F) determines the degree of (θ, ϕ) coupling when angle-tuning parallel to these faces. Such coupling would be essentially zero in the uniaxial limits.

In a given interaction, we can define the actual polarizations at λ_i as $\Delta_i = \delta_i$ or $\Delta_i = \delta_i \pm 90°$, depending on which λ_i eigenmodes are polarized as e_1 and which are polarized as e_2. For uniaxial crystals, the Δ_i are 0° and 90°, respectively, for the e_1 and e_2 polarizations. For biaxial crystals, the Δ_i may vary as much as $\pm 90°$ from these values (locus type AB), but in most cases of practical interest the variation is much smaller (locus type CD and especially EF). We'll discuss further characterization and calculation of the δ_i in the next section.

VIII. Polarization Angles δ_i

The polarization angle δ for eigenmode e_1 in Fig. 1 and e_1, e_2 polarization direction cosines in (1) can be determined analytically [21], [49] or, equivalently, by a geometric construction described in [8], [14], [47], and [48]. The geometric model makes use of two intersecting planes, each formed by the wave vector k and one of the two biaxial optic axes located at angles $\pm\Omega$ to z in the xz plane [13], where

$$\Omega = \pm \arcsin\,[(n_z/n_y)[(n_y^2 - n_x^2)/(n_z^2 - n_x^2)]^{1/2}]. \quad (5)$$

At each wavelength λ_i, δ_i in the Fig. 1(a) and (b) frame is the angle between the internal/external bisectrix of the two aforementioned planes and the plane of the k vector and the "3"-axis, i.e., e_1 is parallel to the sum/difference of the aforementioned plane normals whose z components have the same sign as k_z. Denoting the e_1 polarization angle by δ_i^+ for the Fig. 1(a) frame and by δ_i^- for the Fig.

1(b) frame,

$$\tan 2\delta_i^+ = \frac{\sin 2\phi \cdot \cos\theta}{\sin^2\phi - \cos^2\theta \cdot \cos^2\phi + \cot^2\Omega_i \cdot \sin^2\theta} \quad (6a)$$

$$\tan 2\delta_i^- = \frac{-\sin 2\phi \cdot \cos\theta}{\cos^2\phi - \cos^2\theta \cdot \sin^2\phi + \tan^2\Omega_i \cdot \sin^2\theta}. \quad (6b)$$

Equation (6a) is similar to an expression in [8] and [47], attributed to Tsuboi [48]. The expression in [8] and [47] is, unfortunately, incorrect, due to a typographical error. Equation (6a) has also been derived by Dreger [21].

The uncertainty in evaluating arctan (tan 2δ) when $\delta > 45°$ is resolved by inspection of the aforementioned geometric construction (hint: cut a hole in a pasteboard square, fold it in half, and place it over a similarly sized ball with representative axis markings, such that the fold in the pasteboard represents the k vector). It is seen that δ changes smoothly within each octant and along each Fig. 1 locus (except for propagation down a biaxial axis [14]), and that if we arbitrarily restrict $|\delta_i| \leq 90°$, the sign of δ is given by the sign of the numerator in (6). It can be shown that we must therefore add the similarly signed quantity 180° to arctan (tan 2δ), whenever the denominator in (6) is less than zero, before halving arctan (tan 2δ) to get δ.

Although biaxial e_1, e_2 polarizations are orthogonal for a given wavelength, dispersion in the refractive indexes yields polarizations Δ_i which are not precisely parallel and perpendicular to one another for propagation away from a principal plane. As indicated in Fig. 1, the e_1, e_2 polarizations for biaxial crystals are skewed to uniaxial "e," "o" polarization alignments. This type of skew is zero (uniaxial-like) at locus points B/C/D/E/F, but fully 90° at point A. The skew increases as the k vector moves away from the principle optical planes, except for point A, where the skew decreases monotonically to zero as $k(\theta, \phi)$ proceeds from A towards B along locus AB. Such skew tends to be greater for larger biaxiality [Ω approaching 45° in (5)] and for loci approaching type AB.

IX. Conversion Efficiency

The efficiency for conversion of optical power from one or two of the three interacting waves to the remaining wave(s) can be determined, in the most general situations, by the stepwise, forward integration of the coupled amplitude equations for parametric interactions [55], [56]. These equations require that the incremental power gain/loss at λ_3 be accompanied by a concomitant power loss/gain at λ_1 and λ_2, individually, all of which are in proportion to their photon energies, as expressed mathematically by the Manley–Rowe relation [51]:

$$\mp\lambda_1 \cdot \Delta P_1 = \mp\lambda_2 \cdot \Delta P_2 = \pm\lambda_3 \cdot \Delta P_3 \quad (7)$$

where ΔP_i is the incremental change in power at λ_i. For THG, this implies that one fundamental photon plus one second harmonic photon (twice the power) will, under 100% conversion, yield one third harmonic photon at three times the power. Any imbalance of fundamental or second harmonic photons in excess of this 1:1 ratio will not only be unconverted, but may (like dephasing) lead to back conversion, thus reducing efficiency [43], [69]. For lossless photon-matched interactions only, SFM paraxial conversion efficiency $\eta = I_3/(I_1 + I_2)$ can be approximated to within 0.05 for all drive levels $\eta_o < 20$ and all allowed dephasing $L\Delta k/2$ in the first lobe of the drive-dephasing plane [43], as follows:

$$\eta \approx \tanh^2(\sqrt{\eta_o}) \cdot \frac{\sin^2[L\Delta k \cdot \exp(\eta_o^{0.87}/6.7)/2]}{[L\Delta k \cdot \exp(\eta_o^{0.87}/6.7)/2]^2} \quad (8)$$

where

$$\eta_o = C^2\left(1 + \frac{\lambda_1}{\lambda_2}\right)^2 L^2 \frac{I_1 I_2}{I_1 + I_2}, \qquad I_2\lambda_2 = I_1\lambda_1 \quad (9)$$

and

$$C = 5.454(n_1 n_2 n_3)^{-1/2} d_{\text{eff}}/\lambda_1, \qquad (GW)^{-1/2}. \quad (10)$$

Here, intensities I_i are given in GW/cm^2, wavelengths λ_i in μm, phase-mismatch Δk in cm^{-1}, crystal length L in cm, and effective nonlinear coupling d_{eff} (to be discussed shortly) in pm/V. For SHG, $I_1 = I_2 = I/2$, where I is total input intensity. Equation (8) accounts for input signal depletion and back conversion from drive-enhanced phase mismatch, i.e., when $\Delta k \neq 0$ in (2). For $\eta_o \ll 1$, $\tanh^2(\sqrt{\eta_o}) \approx \eta_o$ and $\exp(\eta_o^{0.87}/6.7) \approx 1$, which reduces (8) to the familiar small signal form $\eta = \eta_o \cdot \text{sinc}^2[L\Delta k/2]$, where sinc $(x) = \sin(x)/x$ [13]. For DFM/OPA/OPO, second lobe behavior, finite losses, and/or photon mismatch, simple analytical approximations such as (8) are usually inadequate, so exact [43], [55] or numerical [69] methods are used.

The phase-mismatch in (8) can be expressed through second order in a change in an arbitrary variable χ by

$$\Delta k = (\partial\Delta k/\partial\chi) \cdot \delta\chi + 0.5(\partial^2\Delta k/\partial\chi^2) \cdot (\delta\chi)^2 \quad (11)$$

where χ could be the (internal) angle θ or ϕ, temperature, wavelength, stoichiometry, or any parameter whose change or variation could cause dephasing of the interaction. Once the conditions for perfect phase matchability ($\Delta k = 0$) have been deduced in (2), first and second-order derivatives of Δk with respect to the chosen parameter χ are easily determined by numerical computation. From these derivatives, we can determine corresponding first- and second-order products $L \cdot d\chi$ and $\sqrt{L} \cdot d\chi$, involving crystal length L and acceptance bandwidth $d\chi$. This is accomplished by calculating Δk for χ incremented by (+) and (−) $\delta\chi$, respectively, (call these Δk values Δk^+ and Δk^-), which are alternately subtracted and summed to get

$$\partial\Delta k/\partial\chi = [\Delta k^+ - \Delta k^-]/[2|\delta\chi|] \quad (12)$$

$$(L \cdot d\chi)_{\text{HWHM}} = 0.886\pi/[\partial\Delta k/\partial\chi] \quad (13)$$

$$\partial^2\Delta k/\partial\chi^2 = [\Delta k^+ + \Delta k^-]/(\delta\chi)^2 \quad (14)$$

$$(\sqrt{L} \cdot d\chi)_{\text{HWHM}} = [1.772\pi/[\partial^2\Delta k/\partial\chi^2]]^{1/2}. \quad (15)$$

The accuracy of such computations is limited by the precision with which the refractive indexes are known with respect to wavelength, temperature, stoichiometry, etc.

One generally ignores second order effects except when the first order term $\partial\Delta k/\partial\chi$ in (11) approaches zero. Such a condition ($\partial\Delta k/\partial\theta = \partial\Delta k/\partial\phi = 0$) is obtained in both uniaxial and biaxial crystals for propagation down a principle optical axis, and is referred to as noncritical phase matching (NCPM). In uniaxial crystals, the NCPM condition is also obtained for propagation in the azimuthal plane in Fig. 1, ($\partial\Delta k/\partial\theta = 0$ at $\theta = 90°$), since $\partial\Delta k/\partial\phi$ is always zero. The latter is not true for biaxial crystals, however, so the condition $\theta = 90°$ in biaxial crystals does not truly represent NCPM unless $\phi = 0°, 90°, 180°$, etc. Nevertheless, angular acceptance with respect to ϕ is often large under this "quasi-NCPM" condition, as is demonstrated by Type II 1064 nm SHG in ZTS [40], LBO and KTP, where external HWHM $L \cdot d\phi = 21$, 9.6, and 7.9 cm-mrad, respectively (see also Table VII). An example of NCPM for phase-matched propagation down the "3" axis in Fig. 1 is temperature-tuned, Type I SHG in LBO [35], [37].

There are very few instances of $\partial\Delta k/\partial\chi = 0$ in uniaxial crystals, other than (angular) NCPM. Such conditions are much more probable in biaxial crystals, because the various $\partial\Delta k/\partial\chi$ vary along the phase-matching loci and may occasionally reach a null value. Hence, for biaxial crystals only, one may have the possibility of choosing a θ, ϕ crystal orientation which optimally compromises d_{eff} and one or more relevant acceptance bandwidths. For instance, it has been shown that deuterated *L*-arginine phosphate (*d*-LAP) has a Type I SHG first-order pole of temperature acceptance [20]. Fortuitously, a maximum in d_{eff} is close by. It should be noted, however, that such calculated results are quite sensitive to the precise form of dispersion in the refractive indexes and thermooptic data used, and may therefore not be observable experimentally. This is particularly true for calculated temperature acceptance poles, since there is a serious paucity of accurate thermooptic data (with accurate wavelength dispersion) in the literature. A general procedure for calculating acceptance bandwidth poles has been given by Dreger [21].

For the special cases of angular sensitivity and angular acceptance bandwidth, one may wish to combine the individual θ and ϕ variables into a single variable A which represents an angular change in the most sensitive direction, i.e., normal to a phase-matching locus in Fig. 1. One may also wish to express angular sensitivity and acceptance bandwidth relative to external rather than internal change in angle. For SFM, we accomplish both objectives as follows:

$$\partial\Delta k/\partial A \approx \left\{\frac{1}{n_1 n_2}\left[\left(\frac{\partial\Delta k}{\partial\theta}\right)^2 + \frac{1}{\sin^2\theta}\left(\frac{\partial\Delta k}{\partial\phi}\right)^2\right]\right\}^{1/2} \quad (16)$$

$$(L \cdot dA)_{\text{HWHM}} = 0.886\pi/[\partial\Delta k/\partial A] \quad (17)$$

with similar versions for DFM_{31}, DFM_{32}, or OPO ($n_3 n_1$, $n_3 n_2$ or n_3^2 instead of $n_1 n_2$). This form is invariant to permutation of the *xyz* frame in which it is computed and is convenient for characterizing arbitrary points along biaxial phase-matching loci. It is also useful for computing (external) "power threshold" [52], not a strict threshold in the traditional sense, but a sophisticated NLO figure-of-merit composed of d_{eff}, sensitivity to (external) angular dephasing, and appropriate wavelengths and indexes of refraction:

$$P_{thr}(GW) = 0.01 \cdot \lambda_1\lambda_2 \cdot [(\partial\Delta k/\partial A)/C]^2. \quad (18)$$

Here, $\partial\Delta k/\partial A$ is in $\text{cm}^{-1}/\text{mrad}$, λ_i is in μm, C is from (10), and P_{thr} denotes a total input power per pulse for efficient conversion η. For a diffraction-limited Gaussian beam of $1/e^2$ radius w_o, whose intrinsic Gaussian divergence is the only source of dephasing, (8) gives $\eta \approx 89\%$ for $I_1 + I_2 = P_{thr}/\pi w_o^2$. This assumes negligible walkoff, that average divergence is equivalent to about $0.4\lambda_1/\pi w_o$ angular detuning, and that the crystal length is chosen for maximum efficiency [again, use (8)].

Note that relative wavelength increments $d\lambda_1$, $d\lambda_2$, $d\lambda_3$ must be taken into account when calculating spectral acceptances in (12)–(15). In Table VII, we arbitrarily size these increments in proportion to the wavelengths (i.e., $d\lambda_1 = 2d\lambda_2 = 3d\lambda_3$, as would be appropriate for THG), but each three-wave situation would have its own inherent constraints, which should be indicated. One should also indicate whether stated acceptance bandwidths are full width half maximum (FWHM), half width half maximum (HWHM) or "peak-to-zero" (PTZ) in the $(\text{sinc})^2$ dephasing factor [13]. One can convert among the three bandwidth (BW) definitions for first- and second-order dephasing as given in (19). It is assumed for (19b) that $\partial\Delta k/\partial\chi = 0$ in (11).

$$\text{first-order: } 2BW_{\text{HWHM}} = BW_{\text{FWHM}} = 0.886BW_{\text{PTZ}} \quad (19a)$$

$$\text{second-order: } 2BW_{\text{HWHM}} = BW_{\text{FWHM}} = 1.331BW_{\text{PTZ}}. \quad (19b)$$

For down conversion processes in which waves are generated from the background noise, multiple parametric contributions can greatly increase apparent acceptance bandwidths over those calculated from (12)–(17), as described by Barnes [57] and Brosnan [58].

X. Double Refraction

It is of interest to determine any mutual angular displacement among the rays in a three-wave interaction as these beams propagate through the crystal. This double-refraction (walkoff) phenomenon will affect conversion efficiency if the rays at some point no longer overlap sufficiently [8], [59], and also has the potential of vignetting

beams whose diameters are comparable to the crystal cross section. Also, calculation of the effective nonlinear coupling d_{eff} requires direction and polarization parameters θ_i^S, ϕ_i^S, δ_i^E for each of the three interacting rays (Poynting vectors $\boldsymbol{S} \perp \boldsymbol{E}, \boldsymbol{H}$), rather than the θ^k, ϕ^k, δ_i^D parameters (our θ, ϕ, δ) for the three (collinear) wave normals $\boldsymbol{k} \perp \boldsymbol{D}, \boldsymbol{H}$ [59]. Failure to make this distinction can result in 0–20% error in calculated d_{eff} maxima, even larger if they are not maxima.

Brehat and Wyncke [60] and Yao and Fahlen [46] have discussed the calculation of ray walkoff in biaxial crystals. We present here a slightly different approach, which yields explicit ray and (nonorthogonal $\boldsymbol{E}$) polarization parameters θ_i^S, ϕ_i^S, $\delta_i^E(m = 1)$, $\delta_i^E(m = 2)$ for later use in the calculation of effective nonlinear coupling, and also lends itself to numerical computation of both absolute and relative ray walkoff.

A unit vector $\boldsymbol{\kappa}$ parallel to the wave normal vector $\boldsymbol{k}$ in our standard Fig. 1 frames is given by

$$\kappa_j = \begin{pmatrix} \sin\theta\cos\phi \\ \sin\theta\sin\phi \\ \cos\theta \end{pmatrix}. \tag{20}$$

Corresponding components N_{ij} of the three (not necessarily collinear) unit Poynting vectors, as a function of the κ_j, the eigenmode indexes n_i and the indicatrix indexes n_{ij} described earlier for (2) and (4), are [14]:

$$N_{ij} = \kappa_j \cdot \frac{1}{\sqrt{1 + h_i}} \cdot \left[1 + \frac{h_i}{1 - n_i^2/n_{ij}^2 + \epsilon^2}\right] \tag{21}$$

where

$$h_i^{-1} = \sum_{j=1}^{3} (\kappa_j^2 + \epsilon)/[1 - n_i^2/n_{ij}^2 + \epsilon^2]^2. \tag{22}$$

The optional terms in ϵ ($\leq 10^{-4}$) are intended to be introduced only when $n_i = n_{ij}$, in order to avoid the indeterminate form $0/0$ and still retain submilliradian accuracy. For rays $i = 1, 2, 3$ and their associated $\boldsymbol{E}$-polarizations, angular counterparts to θ, ϕ, δ_i in (1) are given in the appropriate Fig. 1 POSITIVE OR NEGATIVE NLO FRAME by

$$\text{polar angle: } \theta_i^S = \cos^{-1}[N_{i3}] \tag{23}$$

$$\text{azimuthal angle: } \phi_i^S = \cos^{-1}[N_{i1}/\sin\theta_i^S] \tag{24}$$

polarization parameter:

$$\delta_i^E\,(m = 1) = \sin^{-1}[\sin\delta_i \cdot \sin\theta/\sin\theta_i^S] \tag{25a}$$

$$\delta_i^E(m = 2) = \cos^{-1}[\cos\delta_i \cdot \sin\theta/\sin\theta_i^S]. \tag{25b}$$

Absolute and relative ray walkoff angles are determined by taking scalar products between appropriate pairs of unit vectors $\boldsymbol{\kappa}$, $\boldsymbol{N}_1$, $\boldsymbol{N}_2$, and $\boldsymbol{N}_3$. For example, the absolute walkoff angle $\rho_{3\kappa}$ of the λ_3 ray is given by $\cos\rho_{3\kappa} = \boldsymbol{N}_3 \cdot \boldsymbol{\kappa}$, whereas the relative walkoff angle ρ_{23} between the λ_2 and λ_3 rays is given by $\cos\rho_{23} = \boldsymbol{N}_2 \cdot \boldsymbol{N}_3$. We denote walkoff by the symbol ρ because this is the prevailing uniaxial tradition [59], although this symbol has occasionally been used to denote the polar ray angle θ^S in (23) [13].

In NLO applications where double refraction impacts conversion efficiency, it is the ray(s) with largest walkoff relative to the ray(s) with least walkoff that is usually of most interest. For beam vignetting or offset considerations, absolute walkoff is also of interest. We can accommodate these interests by reporting walkoff of the two rays with largest walkoff relative to walkoff of the ray with least walkoff [60], and reporting walkoff of the ray having least walkoff with respect to the common wave direction. These walkoff angles can be compactly reported for rays $i = (1, 2, 3)$ as, say, (40, *5, 48) mrad, where the starred value indicates the ray with least walkoff. In this example, the eigenmodes are (e_1, e_2, e_1), respectively, so the quasi-"o"-like e_2 eigenmode has the least walkoff (as we might intuitively expect), and the two "e"-like e_1 eigenmodes walk off with respect to the e_2 eigenmode by 40 and 48 mrad, respectively. We will use this format in Table VII (example reporting).

Because biaxial crystals have birefringence in the azimuthal plane in Fig. 1(a) and (b), e_2 walkoff at $\theta = 90°$ (locus point F) isn't necessarily zero, as it would be in the uniaxial limit or as is e_1 walkoff (uniaxial or not). Examples would be (4, *0, 5) mrad for 1064 nm SHG-II in the positive crystal KTP (e_2, e_1, e_2) or (*0, 5, 0) mrad for 1064 nm SHG-II in the negative crystal LBO (e_1, e_2, e_1).

Since the slow/fast eigenmode walkoff planes are the same internal/external bisectrix planes discussed earlier with regard to the polarization angles δ_i and Δ_i [14], dispersion in the refractive indexes implies that the (up to six) walkoff planes in a nondegenerate three-wave interaction will not always be precisely parallel and perpendicular to one another. It can be shown that the effects of dispersion on the otherwise mutual parallelism and orthogonality of these planes are usually weak. The most severe effects (5°–10° discrepancies) would occur midway between locus points A and B for SFM on type AB loci, in which there is significant dispersion in the biaxial optic axes. Even so, since walkoff is generally limited to at most a very few degrees, relative walkoff can always be converted to absolute walkoff by adding it to the minimum (starred) walkoff value if both are in nominally parallel planes, or by using the Pythagorean relation if they are in nominally orthogonal planes.

In Table III, we summarize first octant biaxial walkoff relative to the more familiar uniaxial behavior. Recall that uniaxial e_2 walkoff is always zero, while uniaxial e_1 walkoff is directed toward the "3" axis for positive crystals and toward the "1–2" plane for negative crystals (see Fig. 1).

The descriptions in Table III indicate that, except for the nonzero walkoff for eigenmode e_2 and some skewness in the walkoff directions, there is a good deal of similarity between biaxial and uniaxial walkoff for most situations

TABLE III
CHARACTERIZATION OF FIRST OCTANT WALKOFF FOR e_1, e_2 EIGENMODES IN FIG. 1 NLO REPORTING FRAMES

e_1 Walkoff	e_2 Walkoff
LOCUS A–B Uniaxial-like at B, decreasing to zero at A. Walkoff plane tilts δ_i around $k(\theta, \phi)$, increasing from 0° at B to 90° at A.	LOCUS A–B Zero at B, increasing to a sizable maximum at A. Orthogonal to e_1 walkoff for the same λ_i, pointed increasingly in the direction of positive ϕ for locus points approaching B.
LOCUS C–D Uniaxial-like at C and D, with a moderate-to-large walkoff plane tilt δ_i in between. Tilt δ_i (sense per Fig. 1) is maximum midway between C and D.	LOCUS C–D Zero at C and D, increasing to a maximum midway between C and D. Orthogonal to e_1 walkoff for the same λ_i, and pointed nominally in the direction of increasing ϕ.
LOCUS E–F Uniaxial-like at E, decreasing to zero at F, with a slight-to-moderate walkoff plane tilt δ_i in between. Tilt is maximum midway between E and F.	LOCUS E–F Zero at E, increasing to a small maximum at F. Orthogonal to e_1 walkoff for the same λ_i, and pointed nominally in the direction of increasing ϕ in Fig. 1.

of interest. Locus type AB near point A is the least intuitive with respect to uniaxial behavior. Walkoff in octants 2–8 of the optical indicatrix is determined by successive mirror reflections of first octant behavior across the principal optical planes, i.e., walkoff is completely specified by a single octant, regardless of crystal symmetry.

XI. Effective Nonlinear Coefficient

Conversion efficiency in (8) and virtually all NLO figures-of-merit, such as "power threshold" in (18), contain effective nonlinear coupling d_{eff}, which is a function of the material nonlinear coefficients d_{ijk} and the E-field polarization directions. For SFM, the second-order polarization components $P_r(\lambda_3)$ along rectangular frame axes $r = 1, 2, 3$ can be expressed in terms of the transmitted electric field components $E_p(\lambda_1)$ and $E_q(\lambda_2)$, and the theoretician's second-order susceptibilities $\chi^{(2)}_{rpq}$ or the experimentalist's coefficients d_{rpq} $(= \chi^{(2)}_{rpq}/2)$, as follows [13], [59]:

$$P_r(\lambda_3) = 1/2 \cdot \sum_{p=1}^{3} \sum_{q=1}^{3} \chi^{(2)}_{rpq}(\lambda_3; \lambda_1, \lambda_2) E_p(\lambda_1) E_q(\lambda_2)$$

$$= \sum_{\mu=1}^{6} d_{r\mu}(\lambda_3; \lambda_1, \lambda_2) B_\mu E(\lambda_1) E(\lambda_2) \qquad (26)$$

where symmetry/equivalence considerations permit the $3 \times 3 \times 3$ d_{rpq} tensor to be reduced to the 3×6 contracted form $d_{r\mu}$, and the net $E_p(\lambda_1)E_q(\lambda_2)$ to be proportioned to a 6×1 column vector B_μ. Indexes $\mu = 1, 2, 3, 4, 5, 6$ correspond to $p, q = 1, 1; 2, 2; 3, 3; 2, 3$ (or 3, 2); 1, 3 (or 3, 1); and 1, 2 (or 2, 1), respectively. The column vector B_μ is given by

$$B_\mu = \begin{bmatrix} b_{11} \cdot b_{21} \\ b_{12} \cdot b_{22} \\ b_{13} \cdot b_{23} \\ b_{12} \cdot b_{23} + b_{13} \cdot b_{22} \\ b_{13} \cdot b_{21} + b_{11} \cdot b_{23} \\ b_{11} \cdot b_{22} + b_{12} \cdot b_{21} \end{bmatrix}. \qquad (27)$$

Ray E-field direction cosines b_{ij} in (27) are identical to wave D-field direction cosines a_{ij} in (1), except that the angular coordinates θ, ϕ, δ_i are replaced by θ_i^S, ϕ_i^S, δ_i^E from (23)–(25). There are two possible eigenmodes $m = 1, 2$ for each ray $i = 1, 2$, in (27). In order to accommodate Type I/II/III SFM, DFM, OPA, and OPO interactions, the b_{ij} in (27) must conform to the combination of slow/fast eigenmodes given in Table II for the specified λ_1, λ_2, polarization type and sign of crystal birefringence.

We can project the three polarization components $P_r(\lambda_3)$ in (26) onto the fast eigenmode polarization direction (given by direction cosines b_{3j}) in order to get the net polarization $P(\lambda_3) = d_{\text{eff}} \cdot E(\lambda_1)E(\lambda_2)$ from the total input fields $E(\lambda_1)$ and $E(\lambda_2)$, thereby defining d_{eff} as:

$$d_{\text{eff}} = \sum_{j=1}^{3} \sum_{\mu=1}^{6} [b_{3j} \cdot d_{j\mu} \cdot M_{j\mu} \cdot B_\mu] \qquad (28)$$

where $M_{j\mu}$ is an optional Miller's Rule factor to account for dispersion in the nonlinear coefficients at wavelengths λ_1, λ_2, λ_3 different from the reference wavelengths Λ_1, Λ_2, Λ_3 at which the coefficients were reported [61]:

$$M_{j\mu} = \frac{[n_j^2(\lambda_3) - 1] \cdot [n_p^2(\lambda_1) - 1] \cdot [n_q^2(\lambda_2) - 1]}{[n_j^2(\Lambda_3) - 1] \cdot [n_p^2(\Lambda_1) - 1] \cdot [n_q^2(\Lambda_2) - 1]}. \qquad (29)$$

Contracted index μ is related to p and q as described above.

We are mindful of the admonition of Singh [8] and others to exercise caution in using Miller's Rule for this purpose, especially for monoclinic and triclinic classes, where the orientation of the frame xyz relative to the unequivocal frame XYZ is itself subject to dispersion. Nevertheless, the literature indicates that (29) often gives a good accounting of d_{ijk} dispersion (compare Table V $AgGaS_2$ entries), even near regions of high absorption, and that discrepancies are usually no worse than the 5–20% precision to which the coefficients are typically measured.

Although (26)–(29) are given for SFM, wavelengths λ_3, λ_1, λ_2 may be freely permuted to get similar relationships for DFM and OPO, as long as the Cartesian indexes are permuted with the wavelengths [13], [55], making d_{eff} invariant to interaction type under Kleinman symmetry.

Since NLO conversion efficiency obeys inversion symmetry in addition to crystallographic symmetry, all crystallographic two, four, and sixfold axes become (normals

TABLE IV
ABSOLUTE DETERMINATIONS OF NONLINEAR COEFFICIENT d_{36}(KDP) FOR 1064 nm SHG, AND REFERENCE STANDARDS CHOSEN BY TEXTBOOK/HANDBOOK AUTHORS

Absolute Measurements				
Crystal	λ_1	[Ref]	Scale to KDP for 1064 nm SHG	d_{36}(KDP) (pm/V)
d_{36}(ADP)	633 nm	[62]	TABLE V + CMD	0.41 ± 0.04
d_{36}(KDP)	1060 nm	[63]	NA	0.46 ± 0.04
d_{36}(KDP)	1053 nm	[68]	NA	0.39 ± 0.01
d_{36}(KDP)	1053 nm	[69]	NA	0.39 ± 0.02
d_{36}(KDP)	1053 nm	[70]	NA	0.39 ± 0.04
d_{36}(KDP)	1064 nm	[71]	NA	0.38 ± 0.04
$d_{31}(LiIO_3)$	[parametric]	[64]	TABLE V	0.66 ± 0.10
$d_{33}(LiIO_3)$	[fluorescence]	[66]	TABLE V + CMD	0.63 ± 0.13
Handbook of Lasers (1971), [7]				0.41
Levine and Bethea statistical compilation (1972), [65]				0.44
Applied Nonlinear Optics (1973), [13]				0.46
Landolt-Bornstein (vols. 2, 11, 18, 30; 1969, '79, '84, '92), [11]				0.63
Handbook of Laser Science and Technology (1986), [8]				0.41

to) mirror planes for d^2_{eff}, and vice versa for two-fold axes. Thus, both acentric orthorhombic crystal classes (mm2 and 222) exhibit net mmm and 222 symmetries in this respect, so that the profile of d^2_{eff} along a phase-matching locus is completely specified by just one octant. By contrast, both monoclinic classes (m and 2) exhibit net mirror and two-fold symmetries for d^2_{eff} only with respect to their unique b (= Y) axis. Since there are no other mirror planes, any contiguous 180° rotation around the b axis uniquely specifies d^2_{eff} but 180° contiguous rotations around axes contained in the ac plane must avoid crossing that plane for d^2_{eff} to be completely specified. Such symmetry considerations check the correctness of mathematical algorithms for d^2_{eff} along Fig. 1 loci.

Published (right-hand-frame) nonlinear tensors can be transposed to any other (right-hand) frame by using the transformations found in Appendix III. If the transformation is just a permutation of axes, one need only permute the indices (also works for left-hand-to-right-hand transformations). For instance, in order to transform the 3 × 6 nonlinear tensor for orthorhombic mm2 lithium formate monohydrate from the IEEE/ANSI frame $1'2'3' = XYZ$ to the frame $123 = yzx$, let $1' \rightarrow 3$, $2' \rightarrow 1$, and $3' \rightarrow 2$ in the original frame. Then d'_{31} (= d'_{311}) becomes d_{23} (= d_{233}), d'_{24} (= d'_{223}) becomes d_{16} (= d_{112}), etc., in the transformed frame.

Since NLO figures-of-merit generally involve d_{eff}, theoretical comparisons among different crystals are of limited value unless all d_{ijk} are scaled to a common reference standard. Bechmann/Kurtz [11] and Levine/Bethea [65] were among the first to perform comprehensive reviews of reported nonlinear coefficients and to sort out self-consistent sets of absolute values for both large and small band-gap materials in the face of factors-of-two disparities, differing definitions and various measurement wavelengths in the then available literature. In the next few years, others [63], [64], [66], [67] complemented this work with absolute and relative measurements of like and different materials, using the Constant Miller Delta (CMD) conjecture [61], if necessary, for wavelength scaling. These efforts culminated with accurate determinations of d_{36}(KDP) in the 1980's as a byproduct of the various ICF programs [68], [69], [70], and also with the meticulous work of Eckardt/Byer [71] in 1990. In Table IV, we summarize these different determinations and textbook/handbook recommendations of d_{36}(KDP).

At this writing, the nearly 60% difference between SHG and fluorescence determinations has not been reconciled, although Byer, Kurtz, Tang, and others are trying to resolve this issue (personal communications). Also, disparity between (nonphase-matched) Maker-fringe determinations [45] and phase-matched techniques has not yet been explained (Velsko and Chen, personal communications). In the meantime, we favor the 1064 nm SHG value d_{36}(KDP) = 0.39 ± 0.01 pm/V reported by Eimerl [68], and earlier by Craxton [69]. We believe that the highly characterized ICF lasers used, with their relatively smooth "tophat" spatial profiles, narrow spectral bandwidth, ultralow divergence and sophisticated diagnostics, are better suited for such measurements than most table-top lasers. However, the Nd:YAG and He–Ne lasers used by Eckardt [71] and Francois [62], respectively, were also very well characterized and provide truly independent support of Craxton's and Eimerl's value.

With the above in mind, we summarize in Table V the data of Levine/Bethea [65], Choy/Byer [66], Eckardt/Byer [71] and selected other sources, as indicated, all normalized to d_{36}(KDP) = 0.39 pm/V. We feel that these data lead to a more accurate, self-consistent set of absolute nonlinear coefficients for small and large bandgap materials than previously available, and are tabulated in the right-hand column of Table V. We have indicated by the designations ABS or REL whether the data are absolute, or relative to another material. If the latter, an indication is given of the material and the measurement wavelength, if different from our reporting wavelength, 1.064 μm or 10.6 μm. We have used the CMD conjecture [61] when wavelength scaling is necessary to transform

TABLE V
RECOMMENDED PRIMARY STANDARDS FOR SECOND-ORDER NONLINEAR COEFFICIENTS $d_{i\mu}$ IN IEEE/ANSI FRAME XYZ, USING KLEINMAN'S DEFINITION OF d_{ijk} AND CONDENSED FORM $d_{i\mu}$ [59]. REFERENCED DATA ARE DIRECTLY OR INDIRECTLY PRESCALED TO d_{36}(KDP) = 0.39 pm/V AT 1064 nm SHG (SEE TEXT)

Crystal	$i\mu$	λ_1 (μm)	Data [References]/Comment	This Work (pm/V)
KDP	36	1.064	0.39 [68]–[70]/ABS	0.39
KD*P	36	1.064	0.38 [71]/ABS + REL (KDP); 0.36 [61]	0.37
ADP	36	1.064	0.47 [65], [72]/REL (KDP, SiO2)	0.47
SiO_2	11	1.064	0.30 [65], [72]/REL(ADP, KDP)	0.30
BBO	22	1.064	2.3 [71]/ABS + REL (KDP)	2.3
KTP	d_{eff} (SHG-II)	1.064	3.28 [71]/ABS + REL (KDP) 3.42 [30-update]/REL (KDP) 3.25 [31-update]/REL (SiO_2) @ 0.88 μm	3.3
$LiIO_3$	31	1.064	4.2 [71]/ABS + REL (KDP) 4.4 [66]/REL (KDP-36), $LiIO_3$-33 @ 1.32 μm) 4.7 [73]/REL (KDP)	4.4
$LiIO_3$	33	1.064	d_{33}/d_{31}: 1.00 [66] @ 1.32 μm d_{33}/d_{31}: 1.04 [73] @ 1.06 μm	4.5
$AgGaS_2$	36	1.064	17.3 [74]/REL (SiO2) 17.7/CMD from 10.6 μm average	17.5
$AgGaS_2$	36	10.6	11.1 [74]/REL (GaAs) 11.1/CMD from 1.064 μm average 11.4 [75]/ABS + CMD (1.06/1.29 μm DFM)	11.2
$AgGaSe_2$	36	10.6	37 [66]/REL (LiIO3-33 @ 2.12 μm) 30 [76]/REL (GaAs); 37.4 [77]/ABS 27 [77]/REL (GaAs); 32.4 [67]/ABS]	33
CdSe	33	10.6	37 [66]/REL (LiIO3-33 @ 2.12 μm) 36 [80]/CALC Relative to d_{31}	36
CdSe	31	10.6	16 [78]/REL (GaAs); 20 [79]/REL (d_{33}) 18 [80]/CALC Relative to d_{33}	−18
GaP	36	10.6	37 [65]/REL (SiO2 @ 1.32 μm) 35 [66]/REL (KDP-36, $LiIO_3$-33 @ 1.32 μm) 40 [66]/REL ($LiIO_3$-33 @ 2.12 μm)	37
GaAs	36	10.6	81 [65], 85 [66]/REL ($LiIO_3$-33 @ 2.12 μm)	83

the data to our reporting wavelengths. In the case of Choy/Byer [66], we omitted data employing $LiNbO_3$, preferring instead their measurements relative to d_{36}(KDP) directly, or indirectly via d_{33}($LiIO_3$). Our relative values therefore differ slightly from theirs, in addition to the fact that we've normalized their scale. We chose to discount measurements involving lithium niobate because of data inconsistencies and variability due to stoichiometry, doping and crystal quality.

The Eckardt/Byer listing overlaps the others at key entries (KDP, $LiIO_3$) and adds three new materials: BBO, KTP, and KD*P. Their absolute and relative measurements for these nonlinear materials are self-consistent, and their absolute scale is nearly identical to that in [68]–[70]. Hence, very little scale normalization of their data was required for Table V. A further example of Table V consistency is that the data for $AgGaS_2$ at 1.064 μm, 10.6 μm and intermediate (DFM) wavelengths are mutually consistent via the CMD conjecture. The same data link nonlinear coefficients for small and large bandgap materials GaAs and SiO_2, independently confirming their similar relative sizes in the Levine/Bethea and Choy/Byer scales.

Since most nonlinear coefficients of interest have been measured with reasonable accuracy relative to one of the materials in Table V, we can extend our list of Table V coefficients, as shown in Table VI. Sections III–VI and Appendexes III and IV discuss xyz/abc relationships to XYZ. We omit the remaining KDP isomorphs, since their nonlinear coefficients have been tabulated elsewhere [68].

In those cases where measured data apparently conflict with the Kleinman conjecture [5], the conflicting data are averaged ($KNbO_3$, GMO , CdS, KTP, KTA). Similarly, when there is conflict with Robinson's conjecture [80], we also average appropriately (CdS; see also CdSe in Table V). As a rule, we have as much or more faith in these conjectures than the accuracy of the measurements themselves (typically 5–20%). The coefficients for KTP are perhaps an exception, since [31]-update gives d_{31} and d_{32} 25–30% larger than respective coefficients d_{15} and d_{24}. If true (Kato [30] says not), this would imply that $d_{31} = 4.5$ pm/V and $d_{32} = 2.5$ pm/V in our Table VI (d_{15}, d_{24}, and d_{33} would remain as given). For KTA, [30] and [32] give, respectively, d_{31} and d_{eff} (SHG-II) about $1.3x$ and $1.6x$ greater than for KTP. Hence, we have arbitrarily used $1.45x$ for all Table VI KTA entries. For LBO, we give $d_{i\mu}$ which are most consistent with the SHG/THG d_{eff} maxima, submaxima and zeros in [34], and also best fit the reported loci positions, but which accommodate the ratio d_{33}/d_{31} in [33], as well as (29) THG dispersion. The rms errors for this fit are comparable to those for $d_{i\mu}$ in [34]

TABLE VI
SECOND-ORDER NONLINEAR COEFFICIENTS $d_{i\mu}$ IN IEEE/ANSI STD. 176-1987 FRAME *XYZ* (UNAFFECTED BY OUR PROPOSED AMENDMENT FOR CLASS mm2). THESE VALUES ARE DERIVED FROM GIVEN REFERENCE(S), MODIFIED PER ROBINSON [80] AND/OR KLEINMAN [59], AND SCALED TO TABLE V COEFFICIENTS (pm/V)

Crystal	λ_1 (μm)	[ref]	d_{21} (16)	d_{22}	d_{23} (34)	d_{14} (25, 36)	d_{31} (15)	d_{32} (24)	d_{33}
BBO	1.064	[81], [83]	−2.3	2.3			0.1	0.1	
$BeSO_4$	1.064	[84]				0.22			
BTCC	1.064	[22]					0.08	1.05	1.07
CdS	10.6	[79]					−16	−16	32
d-LAP	1.064	[*]	0.48	0.685	−0.80	−0.22			
GMO	1.064	[23]					−2.6	2.5	−.04
KB5	0.532	[24], [25]					0.04	0.003	0.05
$KNbO_3$	1.064	[27], [28], [30]					−12.8	+11.3	−19.5
KTA	1.064	[30], [32] (see text)					5.2	2.9	12.0
KTP	1.064	[30], [31] (see text)					3.6	2.0	8.3
LBO	1.064	[33], [34] (see text)					0.85	−0.67	0.04
LFM	1.064	[39]					0.13	−0.60	0.94
$LiNbO_3$	1.064	[85] (congruent)	−2.1	2.1			−4.3	−4.3	−27
Urea	1.064	[86]				1.2			
$ZnGeP_2$	10.6	[78]				69			
ZTS	1.064	[40]			—		0.31	0.35	−0.23

*Original *d*-LAP data transformed from 123 = *xyz* to *XYZ* in Appendix III.

and lower than for those in [33]. As in Table I, we note the literature reversals in d_{31} and d_{32} (also d_{15} and d_{24}) for LBO, KTA, KTP, and $KNbO_3$, relative to our IEEE/ANSI notation.

For those classes (tetragonal 4 and 422, trigonal 3 and 32, and hexagonal 6) which have crystallographic symmetry "$d_{14} = -d_{25}$; $d_{36} = 0$," the Kleinman conjecture equates all three coefficients to zero. Support for this conjecture is demonstrated by quartz [88] and $LiIO_3$ [89], where these coefficients are nearly two orders of magnitude less than the principal coefficients. The referenced authors see these nonzero coefficients as a breakdown of the Kleinman conjecture. From a practical standpoint, we view these vanishingly small coefficients as support for the conjecture.

We indicate relative signs of the nonlinear coefficients in Tables V and VI, since absolute signs are usually immaterial in nonlinear optics. The absolute signs have been determined for a number of crystals, however, and are discussed in [8] and [92].

XII. EXAMPLE REPORTING

In order to illustrate the proposed reporting standards, Table VII presents examples of different crystal axialities, polarization types, locus types, and birefringences. Given SHG/SFM wavelengths are chosen in order to maximize the variety, and are not necessarily significant in themselves. Wave vector coordinates θ, ϕ are given in the appropriate Fig. 1 NLO REPORTING FRAME. A (+) or (−) birefringence designation is given after the locus type and/or polarization type under the heading "POLZ-TYPE/LOCUS-TYPE/BIRE-SIGN." For biaxial crystals only, we append the locus designation A, B, C, D, E, or F to the polarization type if phase matching is in a principal optical plane at the corresponding Fig. 1 letter position. Otherwise, we append AB, CD, or EF for an intermediate position on the optical indicatrix, or *x*, *y*, or *z* for propagation down a principal optical axis.

Polarization angles Δ_i are given with respect to the plane of $\boldsymbol{k}$ and the appropriate NLO REPORTING FRAME "3"-axis, under the heading "POLZ ANGLE." The reader is referred to the discussion of double refraction for an explanation of the (starred) absolute walkoff entry versus the two (unstarred) relative walkoff entries, and to the discussion of acceptance bandwidths for constraints pertinent to $L \cdot d\lambda_1$. The angular acceptance bandwidth $L \cdot dA$ is calculated from (17).

In addition to HWHM acceptance bandwidths and d_{eff}, Table VII gives (18) power threshold figure-of-merit (minimum value on locus, except for KTP Type IIE), using the net external angular sensitivity $\partial \Delta k / \partial A$ calculated from (16). In all cases, we have used nonlinear coefficients from Tables V and VI, with (29) for dispersion, and what we believe to be the best refractive indexes and thermooptic data currently available, as referenced in Table VII.

Table VII illustrates the uniform and informative presentation of NLO characteristics using the proposed nomenclature and conventions. No special accommodations (other than Note 1) are necessary for any of the wide variety of polarizations, axialities, loci positions, and birefringences illustrated. Table VII also illustrates the increasingly greater skew polarizations typical of biaxial EF, CD, and AB loci, respectively, and also uniaxial versus biaxial e_1, e_2 walkoff. The importance of considering Type III interactions, as well as traditional Type I and II, is evident for SFM interactions.

TABLE VII
REPRESENTATIVE NLO CHARACTERISTICS, USING PROPOSED STANDARD REPORTING FRAMES AND CONVENTIONS

Crystal [Refs.]	Wavelengths λ_1	λ_2	λ_3	Polz Type, LOCUS Type Bire. Sign.	Polz Angle Δ_1	Δ_2	Δ_3	k-Vector θ	ϕ	Walkoff ρ_1	ρ_2	ρ_3	$\lvert d_{eff}\rvert$	HWHM $\pm L \cdot dA$	HWHM $\pm L \cdot dT$	Note 2 $\pm L \cdot d\lambda_1$	External P_{thr}
	nanometers				degrees			degrees		mrad			pm/V	cm-mr	cm-°C	cm-nm	MW
KDP [90], [91]	1064	895	486	I−	90	90	0	41.4	45.0	*0	0	28	0.27	0.76	5.4	4.72	223
KDP	1064	895	486	II−	0	90	0	56.4	0.0	21	*0	26	0.36	1.30	5.9	2.51	42
KDP	1064	895	486	III−	90	0	0	66.0	0.0	*0	18	21	0.28	1.96	5.7	2.75	30
d-LAP [18]-[20]	1064	895	486	ICD−	83	83	−8	34.3	63.0	0	*7	46	0.79	0.47	8.5	0.76	78
d-LAP	1064	895	486	IICD−	−3	87	−3	40.2	21.2	41	*4	45	0.74	0.83	2.6	0.84	28
d-LAP	1064	895	486	IIICD−	88	−2	−3	45.2	19.4	*4	42	45	0.70	0.97	2.7	0.85	22
LFM [38]	1064	895	486	IAB−	42	42	−48	25.0	73.1	84	84	*54	0.60	0.26	—	0.62	383
LFM	1064	895	486	IIA−	−90	0	−90	7.3	90.0	*0	28	0	0.60	1.38	—	0.61	13.4
LFM	1064	895	486	IIIC−	90	0	0	9.6	0.0	*0	27	29	0.58	1.47	—	0.61	12.6
LFM	980	980	490	IIx−	0	90	0	0.0	0.0	0	0	0	0.61	Note 1	—	0.57	Note 1
LBO [34]-[37]	1318	770	486	IC−	90	90	0	15.6	0.0	*0	0	9	0.83	2.31	2.1	1.68	5.3
LBO	1318	770	486	IID−	0	90	0	73.9	90.0	13	*0	14	0.57	2.28	1.9	1.88	10.7
UREA [87]	1064	895	486	I+	0	0	−90	24.5	0.0	50	50	*0	0.84	0.43	17.2	0.61	72
UREA	1064	895	486	II+	−90	0	−90	34.0	45.0	*0	62	0	0.62	0.63	17.0	0.61	62
UREA	1064	895	486	III+	0	−90	−90	37.5	45.0	65	*0	0	0.68	0.71	17.0	0.61	41
KTP [30], [31]	1318	770	486	ICD+	3	4	−86	48.4	40.2	48	51	*9	0.65	0.43	10.6	0.29	333
KTP	1318	770	486	IID+	−90	0	−90	72.7	0.0	*0	31	0	3.52	1.06	13.7	0.29	1.9
KTP	1064	895	486	IIE+	−90	0	−90	76.2	90.0	*0	22	0	1.99	1.72	8.2	0.24	1.4
KTP	1064	895	486	IIF+	−90	0	−90	90.0	54.6	4	*0	6	2.61	4.96	9.1	0.23	0.1
KB5 [24], [25]	434	434	217	Iy+	0	0	−90	90.0	90.0	*0	0	0	0.04	Note 1	1.1	0.03	Note 1

Note 1: $P_{thr} = 0$, $L \cdot dA = \infty$ to 1st-order when $\partial \Delta k / \partial A = 0$; see [52] and (14), (15) for second-order consideration.
Note 2: Ratio $d\lambda_1 : d\lambda_2 : d\lambda_3$ assumed equal to $\lambda_1 : \lambda_2 : \lambda_3$ for calc. of crystal-length · HWHM-spectral-bandwidth product $L \cdot d\lambda_1$.

XIII. Summary

It is our hope that IEEE/ANSI Std. 176-1987 (amended for orthorhombic class mm2) and other standards summarized below will be adopted by the nonlinear optics community:

1) $\lambda_1 \geq \lambda_2 > \lambda_3$ denote vacuum wavelengths for all interaction types: SHG, SFM, DFM, OPO, OPA.
2) *abc* denotes crystallographic axes (IEEE/ANSI).
3) $\alpha\beta\gamma$ denote interaxial angles (IEEE/ANSI).
4) *XYZ* denotes reporting frame for crystal tensor properties, such as nonlinear $d_{i\mu}$ (IEEE/ANSI).
5) *xyz* denotes principal optic axis frame (traditional).
6) $n_x \leq n_y \leq n_z$ denote refractive indexes for polarization along axes *x*, *y*, and *z* (traditional).
7) 123 = *xyz*/*yzx* = the POSITIVE/NEGATIVE NLO FRAME for θ, ϕ, δ, ρ reporting for POSITIVE/NEGATIVE crystals, where θ is measured from "3" toward the "12" plane and ϕ is measured from "1" toward "2", and where NLO crystal is considered POSITIVE/NEGATIVE according to $\Omega_{ave} \leq 45°$ or $\Omega_{ave} > 45°$ in a given interaction, but either NLO FRAME could be used in marginal cases.
8) I, II, III denote polarization types, per Table II.
9) ABCDEF*xyz* +− denote locus type (Fig. 1 and Table VII).
10) Tables V and VI: $d_{i\mu}$ denote a self-consistent set of nonlinear coefficients based upon d_{36}(KDP) = 0.39 pm/V.
11) Spectral Acceptance: Report $L \cdot d\lambda_1$ (HWHM or FWHM) and indicate assumed constraint ratio $d\lambda_1 : d\lambda_2 : d\lambda_3$.
12) Angular Acceptance: Report net external $L \cdot dA$ as HWHM per (16), (17) or FWHM, or report both $L \cdot d\theta$ and $L \cdot d\phi$ as external HWHM or FWHM (specify which).

We believe that uniform adherence to these conventions would eliminate increasing confusion in the literature and the aggravation of having to transform coordinates in order to compare different works. In order to promote awareness of and distinction among frames *abc*/*xyz*/*XYZ*, we encourage multiple designations for axes and refractive indexes, such as $x = c = Z$ and $n_{x=c}$, or whatever is appropriate. This practice would also minimize potential confusion between lower/upper case designations *xyz*/*XYZ*.

We particularly favor exclusive use of IEEE/ANSI frame *XYZ* for unequivocal reporting of material tensor properties, and also our Fig. 1 "NLO REPORTING FRAMES" for reporting phase-matching loci and eigenmode polarizations, and for characterizing walkoff. The latter frames are traditionally used to characterize uniaxial crystals, and permit simplified perceptions and descriptions of biaxial crystals, using uniaxial behavior as a point of departure. Finally, our updated absolute scale for nonlinear coefficients permit more realistic comparisons of NLO figures-of-merit for both large and small band-gap materials.

Appendix I
Wave Vector θ, ϕ Coordinate Transformation

The following table gives wave vector coordinates θ_N, ϕ_N with respect to the three right-hand permutations of axis assignments "123" in the indicatrix frame *xyz*, given θ_o, ϕ_o in any other permutation. The angle θ is measured from the "3"-axis and ϕ is measured from "1" towards "2." For example, SHG-I for LBO (a negative crystal) has been published as $\theta_o = 90°$, $\phi_o = 11.6°$ in the frame 123 = *xyz* [35], but would be $\theta_N = 11.6°$, $\phi_N = 0°$ in our recommended Fig. 1 NEGATIVE NLO FRAME 123 = *yzx*.

Frame 123		θ, ϕ Transformation
Original	New	θ_O, ϕ_O (Original) to θ_N, ϕ_N (New)
xyz	*zxy*	$\theta_N = \cos^{-1}[\sin\theta_O \sin\phi_O]$
yzx	*xyz*	$\phi_N = \cos^{-1}[\cos\theta_O/\sin\theta_N]$[a]
zxy	*yzx*	
xyz	*yzx*	$\theta_N = \cos^{-1}[\sin\theta_O \cos\phi_O]$
yzx	*zxy*	$\phi_N = \cos^{-1}[\sin\theta_O \sin\phi_O/\sin\theta_N]$
zxy	*xyz*	

[a] If $90° < |\phi_O| < 180°$, change the sign of ϕ_N.

Appendix II
Calculation of Phase-Matching Loci

Yao and Fahlen have given transcendental relationships for Type I/II SHG phase-matched wave normal loci θ, ϕ for the biaxial crystal KTP [46]. Here we generalize these relationships, their (7) and (8), to include Type I/II/III SFM/DFM/OPO in all crystals, as follows:

$$\left(\frac{2/\lambda_3^2}{-B_3 + r_3\sqrt{B_3^2 - 4C_3}}\right)^{1/2} = \sum_{i=1}^{2}\left(\frac{2/\lambda_i^2}{-B_i + r_i\sqrt{B_i^2 - 4C_i}}\right)^{1/2}$$

where their B_i, C_i are evaluated at λ_i in the POSITIVE NLO FRAME. For negative crystals, their results can be transformed to the NEGATIVE NLO FRAME using Appendix I, or obtained directly in this frame by permuting their (k_x, k_y, k_z) to ($\cos\theta$, $\sin\theta \cdot \cos\phi$, $\sin\theta \cdot \sin\phi$). The polarization types in our Table II are accommodated by setting each parameter r_1, r_2, r_3 above to +1 or −1, depending on whether the respective λ_1, λ_2, λ_3 eigenmode is "fast" or "slow."

Appendix III
Tensor Transformation

The nonlinear coefficients d'_{ijk} (rank 3 tensor), traditionally given in IEEE/ANSI frame $1'2'3' = XYZ$, may be transformed to d_{ijk} in any right-hand indicatrix frame 123 = *xyz*, *yzx*, or *zxy* by a 3 × 3 unitary rotation matrix $R_{\alpha\beta}$:

$$d_{ijk} = \sum_{lmn} [R_{il} \cdot R_{jm} \cdot R_{kn} \cdot d'_{lmn}], \quad \text{where}$$

$$R_{\alpha\beta} = \begin{pmatrix} +\cos\psi_1 \cos\psi_2 & +\sin\psi_2 & -\sin\psi_1 \cos\psi_2 \\ -\cos\psi_1 \sin\psi_2 & +\cos\psi_2 & +\sin\psi_1 \sin\psi_2 \\ +\sin\psi_1 & 0 & +\cos\psi_1 \end{pmatrix}.$$

The angles ψ_1, ψ_2 represent a rotation ψ_1 of the frame $1'2'3'$ around $2'$ until $3' = 3$, followed by a rotation ψ_2 around $3'$ until $1' = 1$, $2' = 2$, i.e., until the original $1'2'3'$ frame is coincident with the frame 123. Both rotations are considered positive if counterclockwise when viewing down the rotation axis toward the origin. If this double-rotation can not produce the desired result, an alternate sequence is

$$R_{\alpha\beta} = \begin{pmatrix} +\cos\psi_2 & +\cos\psi_1 \sin\psi_2 & +\sin\psi_1 \sin\psi_2 \\ -\sin\psi_2 & +\cos\psi_1 \cos\psi_2 & +\sin\psi_1 \cos\psi_2 \\ 0 & -\sin\psi_1 & +\cos\psi_1 \end{pmatrix}$$

which represents a rotation ψ_1 of the frame $1'2'3'$ around $1'$ until $3' = 3$, followed by a rotation ψ_2 around $3'$ until $1' = 1$, $2' = 2$. In either case, substituting the transpose matrix $R_{\beta\alpha}$ for $R_{\alpha\beta}$ gives a transformation in the reverse direction.

For example, d-LAP (monoclinic, class 2) has axis equivalences $a = X + 8° = x - 27°$, $b = Y = y$, $c = Z = z - 35°$, near 1064 nm SHG optical frequencies [18]; thus, to transform d_{ijk} (pm/V) in the frame $123 = xyz$ reported in [19] to the IEEE/ANSI frame $1'2'3' = XYZ$ in Table VI, we use the transpose of the first rotation sequence above with $\psi_1 = +35°$ and $\psi_2 = 0°$. In compact notation $d_{i\mu}$, we have (in pm/V)

$$d_{i\mu}^{(xyz)} = \begin{vmatrix} 0 & 0 & 0 & 0.527 & 0 & 0.266 \\ 0.266 & 0.685 & -0.586 & 0 & 0.527 & 0 \\ 0 & 0 & 0 & -0.586 & 0 & 0.527 \end{vmatrix}$$

$$d_{i\mu}^{(XYZ)} \approx \begin{vmatrix} 0 & 0 & 0 & -0.220 & 0 & 0.481 \\ 0.481 & 0.685 & -0.801 & 0 & -0.220 & 0 \\ 0 & 0 & 0 & -0.801 & 0 & -0.220 \end{vmatrix}$$

Similarly, to transform from the frame $1'2'3' = XYZ$ to the NEGATIVE NLO FRAME $123 = yzx$ in Fig. 1(b), we use the first rotation sequence above (not the transpose) with $\psi_1 = +125°$, $\psi_2 = +90°$. In compact notation $d_{i\mu}$, we have

$$d_{i\mu}^{(yzx)} = \begin{vmatrix} 0.685 & -0.586 & 0.266 & 0.527 & 0 & 0 \\ 0 & 0 & 0 & 0 & 0.527 & -0.586 \\ 0 & 0 & 0 & 0 & 0.266 & 0.527 \end{vmatrix}$$

These procedures can be applied to the transformation of other tensor quantities, such as the wave normal vector k_j (rank 1 tensor) or the elastic constants c_{ijkl} (rank 4 tensor) by equating the number of successive matrix operations $R_{\alpha\beta}$ (or $R_{\beta\alpha}$) above to the rank number of the tensor being transformed.

APPENDIX IV
ABBREVIATED IEEE/ANSI Std. 176-1987 AXIS IDENTIFICATION FOR NONCENTROSYMMETRIC CLASSES

This table is provided (with permission) as a convenience to those already familiar with the nomenclature. Reference [4] should be consulted for symbol definitions and important caveats not given here (especially at †), including axis polarity information and possible alternate settings of axes in the plane perpendicular to c for space groups within certain uniaxial point groups (classes).

Crystal System unit cell info	Class	*abc*-Identification			*XYZ*-Identification		
		c	a	b	X	Y	Z
Triclinic $c_O < a_O < b_O$ $\alpha, \beta > 90°$	1					⟨010⟩	c
Monoclinic $c_O < a_O$ $\alpha, \gamma = 90°$ $\beta > 90°$	2 m			2 ⊥m	⟨100⟩ ⟨100⟩	b b	c c
Orthorhombic $c_O < a_O < b_O$ $\alpha, \beta, \gamma = 90°$ (see Note 1)	222 mm2 m2m 2mm	2 2	2 2	2 2	a a c c	b b a b	c c b a
		c	a_1	a_2			
Tetragonal $a_O = b_O$ $\alpha, \beta, \gamma = 90°$	$\frac{4}{}$ $\frac{4}{4}$ 422 4mm $\bar{4}$2m	$\frac{4}{4}$ $\frac{4}{4}$ 4 4 $\frac{4}{4}$	† † 2 ⊥m 2	 2 ⊥m 2	a_1 a_1 a_1 a_1 †	a_2 a_2 a_2 a_2 †	c c c c c
		c	a_1	a_2	a_3		
Trigonal † Hexagonal † $(a_O)_1 =$ $(a_O)_2 =$ $(a_O)_3$	3 32 3m $\frac{6}{}$ $\frac{6}{6}$ 622 6mm $\bar{6}$m2	3 3 3 $\frac{6}{6}$ $\frac{6}{6}$ 6 6 $\frac{6}{6}$	† 2 ⊥m † † 2 ⊥m 2	 2 ⊥m 2 ⊥m 2	 2 ⊥m 2 ⊥m 2	a_1 a_1 a_1 a_1 a_1 a_1 a_1 a_1	 †	c c c c c c c c
		a_1	a_2	a_3			
Cubic $a_O = b_O = c_O$ $\alpha, \beta, \gamma = 90°$	$\frac{23}{}$ $\bar{4}3$m	$\frac{2}{4}$ $\frac{2}{4}$	$\frac{2}{4}$ $\frac{2}{4}$	$\frac{2}{4}$ $\frac{2}{4}$		a_1 a_1	a_2 a_2	a_3 a_3

Note 1: Std. 176-1987 definitions of axes *abc* for the polar orthorhombic class (mm2/m2m/2mm) have not been embraced by the physics and engineering communities. Hence, we recommend that the NLO community and IEEE Standards Board adopt "$Z = c$ = polar (already a *de facto* standard), $X = a$, $Y = b$, $a_O < b_O$." This does not affect *XYZ*, and gives an automatic, convenient, mm2 designation to all crystals in this class.

ACKNOWLEDGMENT

The author would like to thank his colleagues at Cleveland Crystals and Dr. D. Eimerl for their encouragement and helpful discussions; Professor G. C. Bhar, Professor R. L. Byer, Professor C. T. Chen, Professor C. L. Tang, and Dr. K. Kato for their support of the proposed conventions and nomenclature; and Dr. R. S. Craxton, Dr. R. C. Eckardt, and Dr. J. E. Rizzo for their careful critiques of the manuscript. The author would also like to acknowledge the customers of Cleveland Crystals, who have expressed overwhelming support of the standards issue and urged him to put the details of conversations concerning nonlinear optics, conventions, and nomenclature into writing.

REFERENCES

[1] P. A. Franken, A. E. Hill, C. W. Peters, and G. Weinreich, "Generation of optical harmonics," *Phys. Rev. Lett.*, vol. 7, pp. 118–119, 1961.

[2] C. Chen, "Recent advances in nonlinear optical and electro-optical materials," *Ann. Rev. Mater. Sci.*, vol. 16, pp. 203–243, 1986.

[3] "Standards on piezoelectric crystals," *Proc. IRE*, vol. 37, pp. 1378–1395, 1949. This now obsolete standard does not have the same *XYZ* convention for orthorhombic mm2 as the current standard [4].

[4] "IEEE standards on piezoelectricity," IEEE/ANSI Std. 176-1987, esp. ch. 3, "Crystallography applied to piezoelectric crystals," A. W. Warner, D. Berlincourt, A. H. Meitzler, and H. F. Tiersten, pp. 15–28. See Note 1 to Appendix IV for our recommended amendment to this Standard for the polar orthorhombic class mm2.

[5] D. A. Kleinman, "Nonlinear dielectric polarization in optical media," *Phys. Rev.*, vol. 126, no. 6, pp. 1977–1979, 1962.

[6] J. F. Nye, *Physical Properties of Crystals*. London: Oxford Univ., 1957; reprinted with corrections, 1960; the old IRE Std. [3] is cited for axis identifications.

[7] S. Singh, "Nonlinear optical materials," in *Handbook of Lasers*, R. J. Pressley, Ed. Cleveland, OH: Chemical Rubber Co., 1971, Sec. 5, p. 489; the designations *xyz* for the "nonlinear optic axes" on p. 490, *XYZ* for the "piezoelectric axes" on p. 507, and $\alpha\beta\gamma$ for the "principal optical axes" on p. 507 seem to conflict. Singh's updated article in [8] more clearly supports IEEE/ANSI Std. 176 [4], although the old IRE Std. [3] is inadvertantly cited.

[8] S. Singh, "Nonlinear optical materials," in *Handbook of Laser Science and Technology*, M. J. Weber, Ed. Boca Raton, FL: CRC, vol. III: Part 1, Sect. 1.1, 1986, see specific citations [9]and [10].

[9] S. Singh, "Nonlinear optical materials," in *Handbook of Laser Science and Technology*, M. J. Weber, Ed. Boca Raton, FL: CRC, 1986, vol. III; Part 1, Sect. 1.1, p. 53 supports optical *xyz* and IEEE/ANSI *abc* and *XYZ* frames.

[10] S. Singh, "Nonlinear optical materials," in *Handbook of Laser Science and Technology*, M. J. Weber, Ed. Boca Raton, FL: CRC, 1986, vol. III; Part 1, Sect. 1.1, p. 208; Table 1.1.8 supports IEEE/ANSI *abc*, $\alpha\beta\gamma$ and *XYZ* [4], although the table citation is to IRE [3]. The class mm2 axis designation "$z = a, b,$ or c" should read "$Z = a, b,$ or c," a typographical error. See Note 1 to Appendix IV in this paper for our recommended amendment to Std. 176 for designations *a*, *b*, *c* in class mm2.

[11] S. K. Kurtz, J. Jerphagnon, and M. M. Choy, "Nonlinear dielectric susceptibilities," in *Landolt-Bornstein Numerical Data and Functional Relationships in Science and Technology, New Series*, K. H. Hellwege, Ed. Berlin: Springer-Verlag, 1979, Group III, vol. 11, ch. 6; updated from 1969 edition (Bechmann/Kurtz, vol. 2, ch. 5); subsequent update is 1984 edition (Jerphagnon/Kurtz/Oudar, vol. 18, ch. 6); further update scheduled for 1992 (vol. 30).

[12] W. R. Cook, Jr., "Piezoelectric, electrostrictive and dielectric constants, and electromechanical coupling factors of piezoelectric crystals," in *Landolt-Bornstein Numerical Data and Functional Relationships in Science and Technology, New Series*, K. H. Hellwege, Ed. Berlin: Springer-Verlag, 1984, Group III, vol. 18, ch. 3, p. 182; updated from W. R. Cook and H. Jaffe in vol. 11, ch. 3, 1979; further update scheduled for 1992 (vol. 29B).

[13] F. Zernike and J. E. Midwinter, *Applied Nonlinear Optics*. New York: Wiley-Interscience, 1973; the old IRE Standard [3] is cited indirectly through the reference to Nye [6].

[14] M. Born and E. Wolf, *Principles of Optics*. Oxford: Permagon, 1970, ch. 14.

[15] F. A. Jenkins and H. E. White, *Fundamentals of Optics, Fourth Edition*. New York: McGraw-Hill, 1976.

[16] C. S. Hurlbut, Jr. and C. Klein, *Manual of Mineralogy* (after James D. Dana), 19th edition. New York: Wiley, 1977.

[17] S. Umegaki, S. Yabumoto, and S. Tanaka, "Noncollinearly phase-matched second-harmonic generation in $LiIO_3$," *Appl. Phys. Lett.*, vol. 21, no. 8, pp. 400–402, 1972.

[18] D. Eimerl, S. Velsko, L. Davis, F. Wang, G. Loiacono, and G. Kennedy, "Deuterated *L*-arginine phosphate: A new efficient nonlinear crystal," *IEEE J. Quantum Electron.*, vol. 25, pp. 179–193; Feb. 1989; updated nonlinear coefficients (in right-hand frame $123 \equiv xyz$) and thermooptic coefficients can be found in [19] and [20].

[19] S. Velsko, M. Webb, and C. Barker, "Redetermination of nonlinear constants of *d*-LAP," *IEEE J. Quantum Electron.*, to be published.

[20] C. Barker, D. Eimerl, and S. Velsko, "Demonstration of temperature-insensitive phase-matching for second harmonic generation in deuterated L-arginine phosphate," *J. Opt. Soc. Amer., B.*, vol. 8, no. 12, pp. 2481–2492, 1991.

[21] M. A. Dreger, "Temperature insensitive phase-matching for three wave mixing in KTP," R & D Assoc., Albuquerque, NM 87119-9377.

[22] G. Xing, M. Jiang, Z. Shao, and D. Xu, "Bis-thiourea cadmium chloride (BTCC)—A novel nonlinear optical crystal of organometallic complex," *Chin. J. Lasers*, vol. 14, no. 5, pp. 302–308, 1987.

[23] R. C. Miller, W. A. Nordland, and K. Nassau, "Nonlinear optical properties of $Gd_2(MoO_4)_3$ and $Tb_2(MoO_4)_3$," *Ferroelect.*, vol. 2, pp. 97–99, 1971.

[24] H. J. Dewey, "Harmonic generation in $KB_5O_8 \cdot 4H_2O$ from 217.1 to 315.0 nm," *IEEE J. Quantum Electron.*, vol. QE-12, pp. 303–307, May 1976.

[25] Y. Wu and C. Chen, "Calculation of second harmonic generation coefficients of potassium pentaborate tetrahydrate ($KB_5O_8 \cdot 4H_2O$) crystal based on ionic group theory," *Wuli Xuebao*, vol. 35, pp. 1–6, 1986.

[26] W. R. Cook, Jr. and H. Jaffe, "The crystallographic, elastic, and piezoelectric properties of ammonium pentaborate and potassium pentaborate," *Acta Cryst.*, vol. 10, part 11, pp. 705–707, 1957.

[27] Y. Uematsu, "Nonlinear optical properties of $KNbO_3$ single crystal in the orthorhombic phase," *Japan. J. Appl. Phys.*, vol. 13, no. 9, pp. 1362–1368, 1974; our Table VI d_{iu} are based on [27], [28], [30]—update.

[28] I. Biaggio, P. Kerkoc, L. S. Wu, B. Zysset, and P. Gunter, "Refractive indices of orthorhombic $KNbO_3$, Part II: Phase matching configurations for nonlinear optical interactions," *J. Opt. Soc. Amer. B*, vol. 9, no. 4, pp. 507–517, 1992.

[29] F. C. Zumsteg, J. D. Bierlein, and T. E. Gier, "$K_xRb_{1-x}TiOPO_4$: A new nonlinear material," *J. Appl. Phys.*, vol. 47, pp. 4980–4985, 1976.

[30] K. Kato, "Parametric oscillation at 3.2 μm in KTP pumped at 1.064 μm," *IEEE J. Quantum Electron.*, vol. 27, pp. 1137–1140, May 1991. *Update*-personal comm., to be published: d_{eff}(SHG-II) = 3.42 pm/V and $d_{33} \approx 8.3$ pm/V for KTP, with no measurable discrepancy between Kleinman-equal coefficients; $d_{31}(\text{KTA})/d_{31}(\text{KTP}) \approx 1.3$; $d_{31}/d_{32}(KNbO_3) \approx -1.13$, deduced from *yz*-plane d_{eff} null.

[31] J. D. Bierlein and H. Vanherzeele, "Potassium titanyl phosphate: properties and new applications," *J. Opt. Soc. Amer. B*, vol. 6, no. 4, pp. 622–633, 1989. *Update*-personal comm., to be published: $d_{31} = 4.42$, $d_{15} = 3.55$, $d_{32} = 2.38$, $d_{24} = 1.85$, $d_{33} = 16.5$ pm/V (scaled to 1064 nm SHG); our Table V/VI d_{eff}, d_{iu} for KTP are based on [30], [31], [71].

[32] ——, "Linear and nonlinear optical properties of flux grown $KTiOAsO_4$," *Appl. Phys. Lett.*, vol. 54, no. 9, pp. 783–785, 1989; our Table VI d_{iu}(KTA) are based on [32], [30]—update.

[33] S. Lin, Z. Sun, B. Wu, and C. Chen, "The nonlinear optical characteristics of a LiB_3O_5 crystal," *J. Appl. Phys.*, vol. 67, no. 2, pp. 634–638, 1990.

[34] S. P. Velsko, M. Webb, L. Davis, and C. Huang, "Phase-matched harmonic generation in lithium triborate (LBO)," *IEEE J. Quantum Electron.*, vol. 27, pp. 2182–2192, Sept. 1991.

[35] J. T. Lin, J. L. Montgomery, and K. Kato, "Temperature-tuned noncritically phase-matched frequency conversion in LiB_3O_5 crystal," *Opt. Commun.*, vol. 80, no. 2, pp. 159–165, 1990.

[36] K. Kato, "Tunable UV generation of 0.2325 μm in LiB_3O_5," *IEEE J. Quantum Electron.*, vol. 26, pp. 1173–1175, July 1990.

[37] T. Ukochi, R. A. Lane, W. R. Bosenberg, and C. L. Tang, "Measurements of noncritically phase-matched second-harmonic generation in a LiB_3O_5 crystal," *Appl. Phys. Lett.*, vol. 57, no. 10, pp. 980–982, 1990.

[38] S. Singh, W. A. Bonner, J. Potpowicz, and L. G. Van Uitert, "Nonlinear optical susceptibility of lithium formate monohydrate," *Appl. Phys. Lett.*, vol. 17, no.7, pp. 292–294, 1970.

[39] M. Webb and S. P. Velsko, "Phase-matching properties of lithium formate monohydrate for the generation of Nd:YAG harmonics," *IEEE J. Quantum Electron.*, to be published.

[40] H. O. Marcy, L. F. Warren, M. S. Webb, C. A. Ebbers, S. P. Velsko, G. Kennedy, and G. C. Catella, "Second harmonic generation in zinc tris(thiourea) sulfate," *Appl. Opt.*, vol. 31, no. 24, Aug. 1992.

[41] J. E. Midwinter and J. Warner, "The effects of phase-matching methods and uniaxial symmetry on the polar distribution of second-order nonlinear optical polarization," *Brit. J. Appl. Phys.*, vol. 16, pp. 1135–1142, 1965.

[42] M. V. Hobden, "Phase-matched harmonic generation in biaxial crystals," *J. Appl. Phys.*, vol. 38, no. 11, pp. 4365–4372, 1967.

[43] D. Eimerl, "Quadrature frequency conversion," *IEEE J. Quantum Electron.*, vol. QE-23, pp. 1361–1371, Aug. 1987.

[44] S. P. Velsko, "Direct measurements of phase-matching properties in small single crystals of new nonlinear materials," *Opt. Eng.*, vol. 28, no. 1, pp. 76–84, 1989.

[45] J. Jerphagnon and S. K. Kurtz, "Maker fringes: A detailed comparison of theory and experiment for isotropic and uniaxial crystals," *J. Appl. Phys.*, vol. 41, no. 5, pp. 1667–1681, 1970.

[46] J. Q. Yao and T. S. Fahlen, "Calculations of optimum phase match parameters for the biaxial crystal $KTiOPO_4$," *J. Appl. Phys.*, vol. 55, no. 1, pp. 65–68, 1984.

[47] H. Ito, H. Naito, and H. Inaba, "Generalized study on angular de-

pendence of induced second-order nonlinear optical polarizations and phase matching in biaxial crystals," *J. Appl. Phys.*, vol. 46, no. 9, pp. 3992–3998, 1975.
[48] S. Tsuboi, *Henko Kenbikyo (Polarizing Microscope)*. Tokyo: Iwanami, 1965, p. 99.
[49] M. Kaschke and C. Koch, "Calculation of nonlinear optical polarization and phase matching in biaxial crystals," *J. Appl. Phys. B*, vol. 49, pp. 419–423, 1989.
[50] S. W. Xie, X. M. Jiang, Y. L. Chen, and P. J. Wang, "The calculation of optimum phase matching angles for optical parametric oscillation in biaxial crystals," *Ferroelec.*, vol. 94, pp. 143–150, 1989.
[51] J. M. Manley and H. E. Rowe, "General energy in nonlinear reactance," *Proc. IRE*, vol. 47, p. 2115, 1959.
[52] D. Eimerl, "High average power harmonic generation," *IEEE J. Quantum Electron.*, vol. QE-23, pp. 575–592, May 1987.
[53] D. Eimerl, J. Marion, E. K. Graham, and S. Haussuhl, "Elastic constants and thermal fracture of $AgGaSe_2$ and *d*-LAP," *IEEE J. Quantum Electron.*, vol. 27, no. 1, pp. 142–145, Jan. 1991.
[54] D. Hon, "Electrooptical compensation for self-heating in CD*A during second harmonic generation," *IEEE J. Quantum Electron.*, vol. QE-12, pp. 148–151, 1976.
[55] J. A. Armstrong, N. Bloembergen, N. Ducuing, and P. S. Pershan, "Interactions between light waves in a nonlinear dielectric," Phys. Rev., vol. 127, pp. 1918–1939, 1962.
[56] A. Yariv and P. Yeh, *Optical Waves in Crystals*. New York: Wiley-Intersci., 1984.
[57] N. P. Barnes and V. J. Corcoran, "Parametric generation processes: spectral bandwidth and acceptance angles," *Appl. Opt.*, vol. 15, no. 3, pp. 696–699, 1976.
[58] S. J. Brosnan and R. L. Byer, "Optical parametric oscillator threshold and linewidth studies," *IEEE J. Quantum Electron.*, vol. QE-15, pp. 415–431, June 1979.
[59] G. D. Boyd and D. A. Kleinman, "Parametric interaction of focused gaussian light beams," *J. Appl. Phys.*, vol. 39, pp. 3597–3639, 1968.
[60] F. Brehat and B. Wyncke, "Calculation of double refraction walkoff angle along the phase-matching directions in nonlinear biaxial crystals," *J. Phys. B: Atom. Mol. Opt. Phys.* (UK), vol. 22, pp. 1891–1898, 1989.
[61] R. Miller, "Optical second harmonic generation in piezoelectric crystals," *Appl. Phys. Lett.*, vol. 5, no. 1, pp. 17–19, 1964.
[62] G. E. Francois, "CW measurement of the optical nonlinearity of ammonium dihydrogen phosphate," *Phys. Rev.*, vol. 143, no. 2, pp. 597–600, 1966.
[63] W. F. Hagen and P. C. Magnante, "Efficient second-harmonic generation with diffraction-limited and high-spectral-radiance Nd-glass lasers," *J. Appl. Phys.*, vol. 40, no. 1, pp. 219–224, 1969.
[64] A. J. Campillo and C. L. Tang, "Spontaneous parametric scattering of light in $LiIO_3$," *Appl. Phys. Lett.*, vol. 16, no. 6, pp. 242–244, 1970.
[65] B. F. Levine and C. G. Bethea, "Nonlinear susceptibility of GaP; relative measurement and use of measured values to determine a better absolute value," *Appl. Phys. Lett.*, vol. 20, no.8, pp. 272–275, 1972.
[66] M. M. Choy and R. L. Byer, "Accurate second-order susceptibility measurements of visible and infrared nonlinear crystals," *Phys. Rev. B*, vol. 14, no. 4, pp. 1693–1706, 1976.
[67] H. Kildal and J. C. Mikkelsen, "The nonlinear optical coefficient, phasematching, and optical damage in the chalcopyrite $AgGaS_2$," *Opt. Commun.*, vol. 9, no. 3, pp. 315–318, 1973.
[68] D. Eimerl, "Electro-optic, linear, and nonlinear optical properties of KDP and its isomorphs," *Ferroelect.*, vol. 72, pp. 95–139, 1987.
[69] R. S. Craxton, "High efficiency frequency tripling schemes for high power Nd:Glass lasers," *IEEE J. Quantum Electron.*, vol. QE-17, pp. 1771–1872, Sept. 1981; the reported nonlinear coefficient d_{36}(KDP) = 0.78 pm/V agrees with the value 0.39 pm/V in [68] after accounting for the factor of two difference in definition.
[70] L. D. Siebert, KMS Fusion, Inc., Chroma I Nd:Glass ICF laser (personal commun.)
[71] R. C. Eckardt, H. Masuda, Y. X. Fan, and R. L. Byer, "Absolute and relative nonlinear optical coefficients of KDP, KD*P, BaB_2O_5, $LiIO_3$, MgO:$LiNbO_3$, and KTP measured by phase-matched second-harmonic generation," *IEEE J. Quantum Electron.*, vol. 26, pp. 922–933, May 1990.
[72] J. Jerphagnon and S. K. Kurtz, "Optical nonlinear susceptibilities: accurate relative values for quartz, ammonium dihydrogen phosphate, and potassium dihydrogen phosphate," *Phys. Rev. B*, vol. 1, no. 4, pp. 1739–1744, 1970.
[73] J. Jerphagnon, "Optical nonlinear susceptibilities of lithium iodate," *Appl. Phys. Lett.*, vol. 16, no. 8, pp. 298–299, 1970.
[74] G. D. Boyd, H. Kasper, and J. H. McFee, "Linear and nonlinear optical properties of $AgGaS_2$, $CuGaS_2$ and $CuInS_2$, and theory of the wedge technique for measurement of nonlinear coefficients," *IEEE J. Quantum Electron.*, vol. QE-7, pp. 563–573, Dec. 1971.
[75] K. Kato, "High-power difference-frequency generation at 5–11 μm in $AgGaS_2$," *IEEE J. Quantum Electron.*, vol. QE-20, pp. 698–699, July 1984.
[76] G. D. Boyd, H. Kasper, J. H. McFee, and F. G. Storz, "Linear and nonlinear optical properties of some ternary selenides," *IEEE J. Quantum Electron.*, vol. QE-8, pp. 900–908, Dec. 1972.
[77] R. L. Byer, M. M. Choy, R. L. Herbst, D. S. Chemla, and R. S. Feigelson, "Second harmonic generation and infrared mixing in $AgGaSe_2$," *Appl. Phys. Lett.*, vol. 24, pp. 65–68, 1974.
[78] G. D. Boyd, E. Buehler, and F. G. Storz, "Linear and nonlinear optical properties of $ZnGeP_2$ and CdSe," *Appl. Phys. Lett.*, vol. 18, pp. 301–304, 1971.
[79] C. K. N. Patel, "Optical harmonic generation in the infrared using a CO_2 laser," *Phys. Rev. Lett.*, vol. 16, no. 14, pp. 613–616, 1966.
[80] F. N. H. Robinson, "Relations between the components of the nonlinear polarisability tensor in cubic and hexagonal II-VI compounds," *Phys. Lett.*, vol. 26A, no. 9, pp. 435–436, 1968.
[81] C. T. Chen, B. Wu, A. Jiang, and G. You, "A new type ultraviolet SHG crystal β-BaB_2O_4," *Sci. Sinica* (Ser. B), vol. 28, pp. 235–243, 1985.
[82] K. Kato, "Second harmonic generation to 2048 Å in β-BaB_2O_4," *IEEE J. Quantum Electron.*, vol. QE-22, pp. 1013–1014, July 1986.
[83] D. Eimerl, L. Davis, S. Velsko, E. K. Graham, and A. Zalkin, "Optical, mechanical and thermal properties of barium borate," *J. Appl. Phys.*, vol. 62, pp. 1968–1983, 1987.
[84] K. Kato, "High average power UV generation at 0.266 μm in $BeSO_4 \cdot 4H_2O$," *IEEE J. Quantum Electron.*, vol. 26, pp. 1455–1456, Sept. 1990.
[85] R. C. Miller, W. A. Nordland, and P. M. Bridenbaugh, "Dependence of second-harmonic generation coefficients, of $LiNbO_3$ on melt composition," *J. Appl. Phys.*, vol. 42, no. 11, pp. 4145–4147, 1971.
[86] J. M. Halbout, S. Blit, W. Donaldson, and C. L. Tang, "Efficient phase-matched second harmonic generation and sum-frequency mixing in urea," *IEEE J. Quantum Electron.*, vol. QE-15, pp. 1176–1180, 1979; nonlinear, thermo-optic, and original Sellmeier data (updated Sellmeier data in [87]).
[87] M. J. Rosker, K. Cheng, and C. L. Tang, "Practical urea optical parametric oscillator for tunable generation throughout the visible and near infrared," *IEEE J. Quantum Electron.*, vol. QE-21, pp. 1600–1606, Oct. 1985.
[88] G. R. Crane and J. G. Bergman, "Violations of Kleinman symmetry in nonlinear optics: the forbidden coefficient of α-quartz," *J. Chem. Phys.*, vol. 64, pp. 27–29, 1976.
[89] M. Okada and S. Ieiri, "Efficiency in the optical mixing between waves at 1.06 μm and 0.53 μm," *Japan. J. Appl. Phys.*, vol. 10, p. 808, 1971.
[90] F. Zernike, Jr., "Refractive indices of ammonium dihydrogen phosphate and potassium dihydrogen phosphate between 2000 Å and 1.5 μm," *J. Opt. Soc. Amer.*, vol. 54, pp. 1215–1220, 1964.
[91] K. W. Kirby, C. S. Hoefer, and L. G. DeShazer, "Thermooptic coefficients of nonlinear crystals isomorphic to KH_2PO_4," Final Rep., submitted to Lawrence Livermore Lab., 1985. Available from NTIS.
[92] R. C. Miller and W. A. Nordland, "Absolute signs of second harmonic generation coefficients of piezoelectric crystals," *Phys. Rev. B*, vol. 2, pp. 4896–4902, 1970.

David A. Roberts (M'79) was born on September 30, 1939, in Fort Wayne, IN. He received the B.S. degree in physics from the Massachusetts Institute of Technology, Cambridge, in 1961 and the M.S. degree in physics from Case Institute of Technology (now Case Western Reserve University) Cleveland, OH, in 1965.

After completing coursework toward the Ph.D. degree he joined Clevite Research Center, Cleveland. There he worked on the theory and development of monolithic solid-state UHF filters, antireflecting thin film coatings, and the characterization of infrared crystals. In 1973, he co-founded Cleveland Crystals, where he is now Vice President. He has been responsible for the design, engineering, manufacturing oversight, technical support, and customer literature for the company's housed crystal products. These linear, nonlinear, and electrooptic devices have been widely accepted by the commercial laser marketplace and by the international laser fusion (ICF) community.